Structural and metamorphic inheritance controls strain partitioning during orogenic shortening (Kalak Nappe Complex, Norwegian Caledonides).

A. Ceccato[a,1], L. Menegon[a, b], C. J. Warren[c], and A. M. Halton[d]

[a]School of Geography, Earth and Environmental Sciences, University of Plymouth, Plymouth, United Kingdom.

[b]The Njord Centre, Department of Geosciences, University of Oslo, Oslo, Norway

[c]School of Environment, Earth & Ecosystem Sciences, Open University, Milton Keynes, United Kingdom.

[d] School of Physical Sciences, Open University, Milton Keynes, United Kingdom.

[1]Present address: Dipartimento di Scienze Biologiche, Geologiche ed Ambientali, Università di Bologna, Italy

Corresponding author: alberto.ceccato@unibo.it

Authors e-mail: Luca.menegon@geo.uio.no; Clare.warren@open.ac.uk; Alison.halton@open.ac.uk

Keywords: Structural inheritance; Strain partitioning; Kalak Nappe Complex; Norwegian Caledonides; Shear-parallel folds

Abstract

The occurrence of pre-collisional structural and metamorphic fabrics may control the development of new structures during subsequent orogenic deformation. Structural, petrological and geochronological analyses have been performed on selected samples collected along a NW-SE cross section of the Kalak Nappe Complex (KNC) exposed on Kvaløya Island (Finnmark, Norway), in order to define pre-Caledonian or Caledonian affinity of deformation fabrics. Nappes within the KNC experienced different pre-collisional tectonometamorphic histories, resulting in contrasting pre-Caledonian fabrics, which in turn controlled orogen-scale strain partitioning and metamorphic re-equilibration during Caledonian shortening. Caledonian deformation during top-to-SE-directed thrusting occurred at 550-675°C and 0.8-1.0 GPa in the presence of fluid. Suitably-oriented pre-collisional fabrics were firstly exploited as zones of localized shearing internal to the Nappe and subjected to metamorphic re-equilibration during shortening. Fold geometry during Caledonian thrusting was also controlled by the orientation of pre-Caledonian fabrics. SE-verging asymmetric folds were developed after minor tilting of pre-Caledonian upright folds with orogen-parallel hinge in the hinterland consistently with top-to-SE shearing. Shear-parallel folds displaying orogen-perpendicular hinge lines resulted from top-to-SE general shearing of pre-collisional upright folds showing pre-collisional orogen-perpendicular hinge lines. Caledonian metamorphism appears to have been accompanied by infiltration of radiogenic ^{40}Ar-rich fluids, which affected the Ar isotopic system in synkinematic micas.

1. Introduction

Pervasive ductile deformation in the middle and lower crust controls the evolution of the deep portions of orogenic wedges and the accommodation of deep crustal shortening during large-scale thrusting and nappe stacking and folding (Escher and Beaumont, 1997; Williams and Jiang, 2005; Beaumont et al., 2006; Culshaw et al, 2010; Bastida et al., 2014; Wex et al., 2017). During orogenesis, thick-skinned tectonics involves the deformation of crystalline basement units that are commonly characterized by a multi-stage pre-collisional tectonometamorphic history (Audet and Bürgmann, 2011; Faber et al., 2019). The prolonged deformation and metamorphic history of basement units is reflected in the development of multiple and variably oriented fabrics. The occurrence of multiple different fabrics formed under different conditions at different times makes untangling the tectonometamorphic history of basement units very difficult, however this is critical for constraining the different spatial and temporal tectonic processes that take place during either (multiple) orogenic cycles or progressive deformation during the same orogenic cycle. These basement units provide an ideal natural laboratory to analyse how pre-collisional inherited deformation fabrics influence strain accommodation and partitioning during a subsequent orogenic episode (Audet and Bürgmann, 2011; Mouthereau et al., 2013).

Structural inheritance has been shown to affect orogenic shortening both at brittle upper crustal levels (Butler et al., 2006; Massironi et al., 2011; Beltrando et al., 2014; Fossen et al., 2017), as well as at ductile, mid- to lower-crustal conditions (Vauchez and Barruol, 1996; Jammes and Huismans, 2012; Mouthereau et al., 2013). Similarly, pre-collisional metamorphic history may strongly influence the behaviour of basement units during later continental collision, especially those typically characterized by dry and rheologically strong lithologies (Yardley and Valley, 1997; Austrheim, 2013). The definition of the pre-collisional tectonometamorphic history of basement units and related deformation-metamorphic fabrics is therefore of fundamental importance for the analysis and interpretation of strain partitioning and accommodation processes during continental collision. Careful investigations of low-strain domains within nappe complexes can provide information on the different P-T conditions and timing of fabric development, as well as on the geometry of strain. Such analyses are crucial to the understanding of the evolution of polyorogenic basement units and of the role of the pre-collisional history on the architecture of mountain belts (Ridley, 1989; Babist et al., 2006; Kirkland et al., 2006b; Manzotti and Zucali, 2013; Gasser et al., 2015; Faber et al., 2019). In addition, petrological and geochronological analysis of regional-scale fabrics are pivotal for the correlation of deformation stages, the correct interpretation of geochronological age dating and for the inference of orogen-scale tectonic processes (Warren et al., 2012; Skipton et al., 2018).

Here we present the results of field structural, petrological and in-situ $^{40}Ar/^{39}Ar$ geochronological analysis on a NW-SE cross section of the Kalak Nappe Complex (KNC) of the Norwegian arctic Caledonides in the Kvaløya Island (Finnmark, Norway). This cross section exposes polyorogenic units of the KNC that were deformed under mid-lower crustal conditions during the Caledonian orogeny. The units were only partially re-equilibrated and reworked during Caledonian shortening, and therefore preserve large-scale low-strain domains (similar to those reported by Gasser et al., 2015). The studied section is parallel to the Caledonian top-to-SE thrusting direction, and provides an ideal natural laboratory for investigating how pre-collisional fabrics affected the accommodation of increasing strain during shortening. We integrated field observations and structural analysis of different pre- and collisional fabrics with P-T-fluid condition estimates in order to define: (i) the metamorphic evolution of the KNC in the study area, and (ii) how the strain distribution and the geometric style of shortening of a polyorogenic basement nappe depend on the orientation and metamorphic history of pre-collisional fabrics. We find that the KNC nappes underwent two different cycles of tectonometamorphic evolution prior to the Caledonian orogeny. The orientation of the previous fabric affected how strain and metamorphism occurred in the KNC units during the Caledonian collision. The study area shows an abrupt change in orientation of a stretching lineation from *orogen-parallel* to *orogen-perpendicular* towards the foreland. We show that this switch is due to the different orientation of pre-collisional fabrics and of the resulting Caledonian folds, with shear-parallel folds dominating in the foreland part of the section. Finally, we infer that in-situ $^{40}Ar/^{39}Ar$ dates of synkinematic micas from both pre-collisional and collisional fabrics do not directly reflect the timing of crystallization, deformation or cooling related to fabric development or tectonic exhumation. Instead, they appear to have been affected heterogeneously by Ar-rich fluid infiltration during Caledonian metamorphism.

2. Geological setting

The Scandinavian Caledonides formed by the convergence and continental collision between Baltica and Laurentia, which followed the subduction and closure of the Iapetus Ocean, during the Ordovician to Devonian (Roberts, 2003). Ocean closure and continental collision resulted in the stacking of different allochthonous nappes with, from bottom to top, Baltica, Iapetus and Laurentia affinity (Roberts, 2003). Traditionally, the nappe stack has been subdivided into Lower, Middle, Upper and Uppermost Allochthon units (Roberts, 2003; Gee et al. 2008). The deep erosional level of the hinterland of the Scandinavian Caledonides provides direct access to middle- and lower crustal sections subjected to intense collisional deformation and metamorphism in an orogen of Alpine-Himalayan style (Gee et al., 2008).

The geology of the Scandinavian Caledonides in Finnmark, northern Norway, consists of windows of Baltica basement with its metasedimentary autochthonous units, overlain by parauthochtonous metasediments (Fig. 1a) (Roberts, 2003). Above the parautochthonous units, the stack of allochthonous nappes that were thrusted eastward over Baltica is dominated by the Kalak Nappe Complex (KNC), a composite nappe pile consisting of several different thrust sheets telescoped onto Baltica during the Caledonian Orogeny (Corfu et al., 2007; Kirkland et al., 2007b; 2008b). The KNC represents a section of reworked middle and lower continental crust that had previously experienced several Neoproterozoic events prior to the Caledonian Orogeny (Sturt et al., 1978; Daly et al., 1991; Kirkland et al., 2005; 2006a; 2007a, 2007b; 2008a; 2008b; Corfu et al., 2011; Gasser et al., 2015; Gee et al., 2017), when it was subjected to pervasive deformation and metamorphism during nappe stacking (Gasser et al., 2015; Faber et al., 2019).

2.1. Geology of the Kalak Nappe Complex

The KNC is composed of ortho- and paragneisses, metasediments of psammitic and pelitic composition and variably affected by migmatization, minor schists and marbles, and felsic and mafic intrusive rocks (Zwaan and Roberts, 1978; Rice, 1990). These lithologies are variably grouped and distributed in two distinct polyorogenic crustal sections that form the lower and the upper nappe of the KNC (Kirkland et al., 2006b). The two nappes are further subdivided into different internal units and thrust sheets (Kirkland et al., 2008b).

The lower nappe includes the Fagervik gneissic complex, predominantly composed of quartzo-feldspatic gneisses and amphibolites, and the overlying metasediments of the Sværholt succession (Kirkland et al., 2008b). Detrital zircon ages of 1948 ± 17 Ma reveal a Paleoproterozoic age for the protolith of the Fagervik gneisses (Kirkland et al., 2008b). Partial melting and emplacement of granitic intrusions in the Fagervik complex occurred at 1796 ± 3 Ma. These ages are consistent with the origin of the Fagervik complex as Baltica basement (Kirkland et al., 2008b). The depositional age of the Sværholt succession is bracketed by detrital U-Pb zircon ages between 1030 and 980 Ma. The sediments were affected by late Grenvillian metamorphism, deformation and partial melting at 980-960 Ma (Kirkland et al., 2006a; 2007b). The contact between the two units is probably of tectonic origin, as supported by recent studies on zircon provenance (Kirkland et al., 2007b, 2008b).

The upper nappe is composed of paragneisses and metasediments of the Sørøy succession, which includes the Eidvågeid series (dominated by migmatitic paragneisses), the Klubben psammites, and the Storelv schists (Kirkland et al., 2005). The Sørøy succession was deposited between 910-840 Ma (Kirkland et al., 2007b), and was deformed, metamorphosed and intruded by granitic melts during the Porsanger Orogeny at c. 850-820 Ma and during the Snøfjord event at c. 710 Ma (Kirkland et al., 2006a, 2006b, 2007b; Corfu et al., 2007; Gasser et al., 2015).The Sørøy succession was also intruded and locally migmatised and deformed between 580-520 Ma by the Seiland Igneous Province (SIP), a series of mafic to ultramafic and alkaline intrusions related to the rifting of the Iapetus Ocean (Daly et al., 1991; Elvevold et al., 1994; Roberts et al., 2006; Menegon et al., 2011).

The exact timing and the origin of the juxtaposition between the lower and the upper nappe of the KNC are still debated (e.g. Corfu et al., 2007). It has been suggested that the original unconformity (now tectonized) between the underlying Sværholt succession and the overlying Sørøy succession is preserved on Hjelmsøy (Kirkland et al., 2008b), and that the juxtaposition was pre-Caledonian, as both successions were affected by the c. 710 Ma Snøfjord tectonomagmatic event (Kirkland et al., 2006a).

The internal structure of the KNC has been traditionally described to result from several discrete deformation stages ("5 or 6 folding events" of Zwaan and Roberts, 1978; Rhodes and Gayer, 1977; Rice, 1998) during Neoproterozoic and Caledonian orogenesis. Gayer et al. (1985) and Kirkland et al. (2006b) identified 5 deformation stages (D_1 – D_5) based on fold geometry and orientation, and on crosscutting relationships between fabrics and granitic intrusions of known age. Whilst D_1 is only very rarely preserved, D_2 is widely preserved in both the lower and upper nappe of the KNC (Kirkland et al., 2006a). U-Pb zircon dating of magmatic intrusions, and their structural relationship with the D_2 deformation fabrics, suggest that D_2 deformation was diachronous and occurred at different times within each nappe of the KNC (Kirkland et al., 2006a). D_3 is generally referred to as the main Caledonian deformation stage in the KNC, which resulted in the formation of the regional foliation during the collisional stage of the orogeny (i.e. the Scandian stage: Roberts, 2003; Gasser et al., 2015; Faber et al., 2019). D_4 and D_5 represent late-Caledonian crenulation and gentle folding of the main regional foliation.

However, regional correlation of structures and their attribution to regional scale, discrete deformation stages is difficult without accurate geochronological and petrological constraints on the age and metamorphic conditions of fabric development (Fossen et al., 2019). In addition, several of the traditionally described “deformation stages” deduced from the different fold orientation and from the superposition of fold geometries may effectively result from progressive deformation during a single tectonic event (Fossen et al., 2019). Therefore, in the present work, the observed structural features are first described in terms of their geometry, orientation and metamorphic mineral assemblages, and then their possible allocation to regional-scale tectonic events is discussed.

3. Methods

Petrographic and microstructural analysis were performed using polarized light- and scanning electron microscopy (SEM) on oriented polished thin section cut parallel to the stretching lineation and perpendicular to the foliation. SEM analysis was conducted with a JEOL 6610

SEM at the Electron Microscopy Centre of the University of Plymouth. Electron microprobe analyses were performed at the Open University (Milton Keynes, UK) and at the Department of Lithospheric Research of the University of Vienna (Austria) with a WDS CAMECA SX 100 equipped with five WDS spectrometers.

Sample preparation and bulk chemical XRF analyses were performed at the Consolidated Radio-isotope Facility (CoRIF) at University of Plymouth with a WDS XRF PANalytical Axios Max spectrometer (fused bead prepared using a PANalytical Eagon 2 fusion system).

P-T conditions of selected samples were estimated by calculating phase diagram sections with Perple_X (Connolly, 2005) using the internally consistent thermodynamic database of Holland and Powell (2011). The pseudosection were calculated for the MnO_2-Na_2O-CaO-K_2O-FeO-MgO-Al_2O_3-SiO_2-H_2O chemical system. Table SM1 reports the list of solid solution models used and the independent end-members with abbreviation from Perple_X. Modal proportion and chemical compositions of solid solutions were defined as follows: (i) albite component of Pl(h) model, X_{Ab}= Na/(Na+Ca); (ii) Mg# of Bi(W), Mica(W), Gt(W): Mg# = Mg/(Mg+Fe^{2+}) in molar proportions; Ti, Fe^{3+} and Mn components of biotite were neglected; (iii) molar fractions of grossular, spessartine, almandine of garnet as X_{Grs}, X_{Sps} and X_{Alm} components of Gt(W) solid solution and Mg# = Mg/(Mg+Fe^{2+}+Mn). Amphibole-plagioclase geothermobarometry was applied to pairs of amphibole and plagioclase grains in contact with each other to estimate the temperature and pressure of fabric development using the methods of Holland and Blundy (1994) and Bhadra and Bhattacharya (2007).

In-situ UV Laser $^{40}Ar/^{39}Ar$ geochronology was carried out at the Open University, UK, on polished 200 µm-thick polished sections from samples 240 and 251. Analyses were carried out on a Nu Instruments Noblesse Mass Spectrometer coupled to a Photon Machines Excite 193 nm laser. Analysis involved ablation of 65 µm to 85 µm spots in the biotite and muscovite grains, after which gases were cleaned with 2 SAES AP-10 getters running at 450°C and room temperature. Detailed description of analytical conditions and data processing for all analytical techniques can be found in the Supplementary Material.

4. Field observations: the Kalak Nappe Complex on Kvaløya

4.1. Lithologies and tectonostratigraphy

The map of the study area (Fig. 1b) is a revision of existing map material (1:50000 Hammerfest sheet: Jansen et al., 2012) based on our field observations. The lower nappe on Kvaløya (Fig. 1b-c) is mainly composed of: (i) the Fagervik gneissic complex, (ii) metasediments of the Sværholt succession (metapsammites/metapelites), and (iii) an undifferentiated banded gneiss unit, composed predominantly of high-grade metapelites, amphibolites and metapsammites. The Fagervik complex (Fig. 2a-b) is characterized by distinctive banded quartzo-feldspathic gneisses intercalated with amphibolites and with rare ultramafic layers and pods. Quartzo-feldspathic gneisses include paragneisses, and orthogneisses, locally showing mylonitic fabrics. Up to 2 metres thick bands of garnet-rich amphibolites are common (Figs. 2b, SM1a). The metasediments of the Sværholt succession are dominated by metapsammites and minor biotite-rich metapelites (Fig. SM1b). The banded gneiss unit has a distinctive rusty colour on outcrop and includes different lithologies arranged in bands that range in thickness from < 5 cm to 1-2 m (Fig. 2c). The most common lithologies of this unit are quartzites, psammites, high-grade (aluminosilicate-bearing) micaschists, migmatitic garnet- and biotite-rich schists, and garnet-rich amphibolites (Fig. SM1c). The banded gneiss unit is laterally discontinuous, and it is observed at both contacts between the lower- and the upper nappe (Fig. 1b).

The Fagervik complex is the lowermost unit of the area and represents the base of the lower nappe. We grouped the “rusty” banded gneiss unit together with the Fagervik complex, based on the occurrence of distinctive layers of garnet amphibolites of similar thickness in the two units (Fig. SM1a,c), and on the consistent structural style displayed by all lithologies (see next chapter). Furthermore, the Fagervik gneisses and the banded gneiss units show a strong lithological affinity with the Fennoscandian (Baltica) basement, such as the West Troms Basement Complex as described in Bergh et al. (2014) and Gee et al. (2017).

In the study area, the upper nappe is dominated by the migmatitic paragneisses of the Eidvågeid Series (Rice and Roberts, 1988; Rice, 1990; Corfu et al., 2007; Gasser et al., 2015; Faber et al., 2019), with minor bands of psammites tentatively correlated with the Klubben psammite (Fig. 1b). Stromatic migmatites are defined by up to 10-20 cm thick quartzo-feldspatic leucosomes alternating with biotite-sillimanite-rich melanosome. The migmatites contain large clusters and individual crystals of dark pink garnet (up to 10 cm in diameter), typically surrounded by thin (< 1 cm thick) feldspar-rich rims. The unit also contains intercalated minor bands of calcsilicates and marbles, as well as several pegmatitic intrusions predominantly discordant to the stromatic banding. Towards the boundary with the lower nappe, migmatitic paragneisses make transition to muscovite-rich paragneisses and minor schists. These rocks contain up to 2-3 cm long mica-fish of muscovite and dark pink garnet porphyroclasts. The stromatic migmatites and the muscovite-rich paragneisses are intercalated with more psammitic bands ranging in thickness from ≤ 5 m to about 50 m.

4.2. Structural domains

Along the analysed NW-SE cross section in Kvaløya, the KNC can be subdivided in three main areas, where the lower- and the upper nappe show different structures and internal deformation features (Fig. 1b, d). In northern Kvaløya, the lower nappe is characterized by NE-SW trending folds and by subhorizontal NE-SW trending stretching lineations parallel to fold axes (Lower nappe North, Fig. 1d). The upper nappe is exposed in central Kvaløya, where foliations are generally also striking NE-SW and contain NE-SW-trending stretching lineations (Upper nappe, Fig. 1d). The lower nappe occurs again in southern Kvaløya, where it is characterized by a dominant shallowly NW-dipping foliation that envelops low-strain domains where NW-SE-trending upright folds are observed (Lower nappe South, Fig. 1d). The contact zone between the upper nappe and the lower nappe is exposed near the localities of Rypefjord (northern contact zone, NCZ in Fig. 1b) and, more continuously, at Grotnes (southern contact zone, SCZ in Fig. 1b). The SCZ develops over a distance of 1 km and consists of a high strain zone with a foliation shallowly dipping to the NW. Our observations and analysis of the contact zone predominantly come from this area.

4.3 Structures in the lower nappe

In the lower nappe the main foliation is defined by a gneissic banding (S_G), which is folded by upright, NE-SW trending, open to tight mesoscopic folds that form the dominant structural pattern of the lower nappe in northern Kvaløya (Figs. 2a-b, SM1a-b). No axial plane foliation is associated with upright folds. Elongated trails of white mica and amphibole, and feldspar- and quartz-rods, delineate a fold-axis parallel stretching lineation (Figs. 1d, 2b). The average orientation of the stretching lineation is 06°/045° (plunge/trend), and this will be referred to as *orogen-parallel* stretching lineation hereafter (Fig. 1d). This stretching lineation is locally associated with a dextral kinematics (Fig. 2d).

Locally, upright folds display a weak top-to-SE tilting (see the dispersion of poles to axial plane in Fig. 1d; Figs. 2a, SM1b). ANW-SE-trending stretching lineation locally develops on NW-dipping fold limbs (average orientation: 39°/310°; see scatter red dots in stereonet Lower Unit North in Fig. 1d). Mesoscale fold asymmetry is consistent with the occurrence of a regional scale SE-vergent synform (β-axis: 04°/247°; fold axial plane: 44°/333°, dip/dip direction) (Fig. 5a-b; Sturt et al., 1978; Akselsen, 1982).

On southern Kvaløya, the lower nappe is characterized by a dominant shallowly NW-dipping foliation (S_{main}: 27°/312°), wrapping around local low-strain domains (Figs. 1d, 3a-e). The main foliation locally shows mylonitic fabric, with the development of sheath folds (Fig. 3b), and kinematic indicators indicating top-to-SE transport (Fig. 3c). Within low-strain domains, NW-SE-trending upright folds with subhorizontal fold axis are preserved and are similar to the upright folds cropping out on northern Kvaløya. However, upright folds on southern Kvaløya are oriented almost normal (fold axis orientation: 10°/340°) to the upright folds on northern Kvaloya (Fig. 1d). In the low-strain domains, Type-3 refolded fold geometries (Ramsay, 1962; Grasemann et al., 2004) are observed. The extent of refolding of upright folds within low-strain domains varies from gentle (with the development of crenulated upright folds with subhorizontal axial planes: Fig. 3d) to tight (with the development of tight, recumbent folds: Fig. 3e). In all cases, the fold axis of re-folded folds is almost parallel to the stretching lineation developed on the main foliation planes (fold axis: 15°/322°; stretching lineation: 26°/329°, Fig. 1d) and defined by elongated trails of white mica, amphibole and biotite, and by rods of quartz and feldspar. Thus, the re-folded folds in southern Kvaløya can be classified as *shear-parallel* folds (Xypolias et al., 2013). In summary, the main foliation is axial planar to re-folded folds and contains a NW-SE trending stretching lineation associated with a top-to-SE kinematics (Figs. 1d, 3b-c). This stretching lineation in Southern Kvaløya is hereafter referred to as *orogen-perpendicular* lineation.

4.4. Structures in the upper nappe

The NNE-SSW-trending stromatic migmatite banding defines the oldest fabric in the Eidvågeid Series (S_{mig}). It is mostly steeply dipping, but the dip angle can vary to define small and large-scale NE-SW trending folds (Figs. 1d, 4a). Mylonitic shear zones are frequent in the Eidvågeid migmatites, and appear as fine-grained, light purple rocks with cm-sized euhedral dark pink garnets surrounded by quartzo-feldspathic rims (Fig. 4b). The main mylonitic foliation S_m (shallowly NNW-dipping) is a mm-cm scale compositional banding between alternating biotite-sillimanite-rich layers and quartzo-feldspathic domains (Fig. 4b). S_m contains a NE-SW-trending stretching lineation L_m (parallel to the axis of the NE-SW trending folds) defined by rodding of feldspar and quartz and by elongate trails of sillimanite. In relatively low-strain domains, S_m represents a crenulation cleavage foliation from folding of the S_{mig} in the stromatic migmatites, locally defining an anastomosing pattern of shear zones with a strong stretching lineation ("coaxial network" of shear zone of Fossen and Cavalcante., 2017) (Fig. 4c). No consistent systematic shear sense indicators have been observed in the mylonitic shear zones, and both dextral and sinistral kinematics exist.

4.5. The Contact Zone

The NCZ between the lower and the upper nappe dips to the NW from shallowly to steeply and juxtaposes a sequence of banded gneisses with the muscovite-rich Eidvågeid paragneisses (Fig. 1b). This geometry results from parasitic folding to the regional-scale SE-vergent synform (Fig. 5a-b). The stretching lineations are invariably subhorizontal and oriented NE-SW in both units, parallel to the fold axes in the area (Fig. 1d).

The SCZ (Fig. 1b) is characterized by a sequence of different lithologies that includes, from north to south: (i) Eidvågeid migmatites with a mylonitic foliation (S_m), intercalated with psammitic layers; (ii) fine-grained banded mylonites with metapelitic Grt + Wm + Sill layers alternating with amphibolite bands, locally including symmetric boudins of pegmatites; (iii) muscovite-rich Eidvågeid paragneisses with large (up to 3 cm) Wm fishes and dark pink garnet; (iv) micaschists, amphibolites and garnet amphibolites presumably belonging to the banded gneiss unit. Foliations are consistently shallowly NW-dipping in the southern contact zone (27°/311°). Lithology (i) display the *orogen-parallel* L_{Sm} lineation. Lithology (ii) marks the sharp onset of the occurrence of *orogen-perpendicular* NW-SE trending lineation associated with top-to-SE kinematic indicators (lineation: 26°/329°; Figs. 1d, 4d-e). The stretching lineation is subparallel to the fold axis preserved in low strain domains between mylonitic high-strain zones (Fig. 3a). Lithology (ii) is interpreted as a tectonic sliver of the lower nappe incorporated into the original contact zone between the two nappes.

5. Microstructure and P-T conditions of fabric development

Based on the structural and tectonostratigraphic constraints derived from the field observations, we selected the following samples for the determination of the P-T conditions of fabric development (Figs. 1b and 5a-b):

- Sample 360 (marked as 1), representative of the pre-Caledonian main fabric in the ‘rusty’ banded gneiss unit of the Fagervik complex (lower nappe). The foliation is oriented 42°/304° and contains a subhorizontal NE-SW stretching lineation (05°/036°).

- Sample 240 (marked as 2), representative of the pre-Caledonian S_m fabric in the mylonitic Eidvågeid Series (upper nappe). S_m in sample 240 is oriented 40°/311° and contains a stretching lineation oriented 03°/042°.
- Sample 251 (marked as 3), representative of the main fabric associated with Caledonian top-SE deformation in the muscovite-rich Eidvågeid paragneisses (upper nappe - SCZ). The main foliation is oriented 12°/307° and contains a stretching lineation oriented 24°/304°.
- Samples 372 and 367 (marked as 4 and 5, respectively), representative of the main fabric associated with Caledonian top-SE deformation in the Fagervik complex (lower nappe). The main foliation in sample 372 dips 35°/306 and contains a stretching lineation oriented 24°/356°. The main foliation in sample 367 is oriented 25°/320° and the lineation plunges shallowly to the NW (17°/341°).

Sample locations are reported in Table SM2. XRF bulk rock compositions are reported in Table 1. Mineral compositions obtained from EMP analysis are reported in Table 2. P-T pseudosections were calculated for the metasediment samples 240, 251, and 360. Amphibole-plagioclase geothermobarometry was applied to constrain the conditions of fabric re-equilibration in amphibolites from the Fagervik complex (samples 367 and 372). Results are reported in Table 3. Mineral abbreviation after Whitney and Evans (2010).

5.1. Main foliation with top-to-NE kinematics in the lower nappe

The mineral assemblage consists of quartz (Qtz), plagioclase (Pl), K-feldspar (Kfs), biotite (Bt), white Wm (Wm), sillimanite (Sill), garnet (Grt), titanite (Ttn) (Fig. 6a). The main Bt + Wm foliation envelops isolated asymmetric Wm fish and Kfs porphyroclasts that indicate a dextral sense of shear (Fig. 6a). Relict grains of sillimanite elongate parallel to the foliation are replaced by white Wm (Fig. 6b). Recrystallized Pl in the matrix has a homogeneous composition (Ab_{79-81}). Mg# in Bt ranges between 0.46 and 0.49. Mg# and Si content of Wm in the recrystallized matrix ranges between 0.62-0.65 and 6.29-6.35, respectively. Wm fish display homogeneous composition (Si=6.27 a.p.f.u., Mg#=0.60). Idioblastic Grt shows homogeneous composition (Alm_{75-77} Grs_{7-8} Prp_{12-14} Sps_2; Mg# = 0.14-0.16) and it grows in isolated pockets, showing commonly euhedral rims and Qtz + Ttn + Bt + Sill inclusion-rich cores.

The P-T pseudosection was calculated using a H_2O amount of 1.78 wt%, as obtained from LOI measurement. The phases identified in the sample are not predicted to be stable at any P-T conditions within the investigated range (Fig. 7a). Considering Kfs and Sill porphyroclasts as relict/metastable phases, the stable mineral assemblage should include Qtz + Pl + Wm + Bt + Grt. This mineral paragenesis is stable over a wide range of P-T conditions. However, Pl (X_{Ab}) and Grt isopleths (Mg#, X_{Grs}) suggest that Grt growth occurred at T=500-550°C and P=0.62-0.72 GPa. The stable mineral assemblage at these conditions consists of Qtz + Grt + Bt + Pl + Wm ± kyanite (Ky) ± staurolite (St) (Fig. 7a-b). Ky and St are expected to occur in very low amounts (<2 vol%). Mg# of both Bt and Wm are calculated to be stable at similar pressure conditions but slightly higher temperature . Sill and Kfs are stable together only at higher temperature (>650°C) and pressures <0.7 GPa; where the aluminosilicates content becomes significant (~10 vol%).

5.2. S_m fabric in the upper nappe: mylonitic Eidvågeid migmatite

The mineral paragenesis consists of Qtz + Pl + Bt + Grt + Kfs + rutile (Rt) + oxides (Ox) + zircon (Zrn) + monazites (Mnz) (Fig. 6c). The sample displays a coarse-grained (50-100 μm) Qtz + Bt + Kfs mylonitic foliation, with sub-mm-size plagioclase porphyroclasts and garnet porphyroblasts (Fig. 6c-d). Kfs is mainly observed as interstitial phase forming thin films around Pl and Grt crystals (Fig. 6e). Recrystallized Pl in the matrix has a homogeneous composition ($Ab_{61\text{-}66}$). Mg# in Bt ranges between 0.53 and 0.56. Grt shows a homogeneously distributed large inclusions of Qtz, Bt and Rt. Grt rim compositions are slightly enriched in grossular ($Alm_{65\text{-}74}$ $Grs_{10\text{-}16}$ $Prp_{14\text{-}19}$; Mg# = 0.16-0-20) compared to the more pyrope-rich core compositions ($Alm_{67\text{-}73}$ $Grs_{4\text{-}6}$ $Prp_{20\text{-}25}$; Mg# = 0.21-0.26).

P-T pseudosection for sample 240 has been calculated for a constant H_2O amount of 0.51 wt%, as obtained from LOI measurements. The observed mineral paragenesis is stable over a large range of P-T conditions. However, the intersection of Bt, Pl isopleths and the composition of Grt cores suggests the likely stability of this paragenesis at 725-750°C and 0.62-0.83 GPa (Fig. 7c-d). The stable mineral assemblage at these conditions consists of Melt + Qtz + Bt + Pl + Kfs + Grt + Sill. The lack of Wm indicates that deformation occurred at pressure <0.78 GPa. X_{Grs}-rich Grt rims suggest lower temperature and higher pressure conditions for re-equilibration (T~500-700°C, P~0.72-1.08 GPa), although this Grt composition is not stable with the measured compositions of Bt and Pl. Considering a bulk H_2O content of 0.51 wt%, H_2O is not expected to be stable as a free phase in the wide range of P-T conditions modelled here (Figs. 7c-d).

5.3. Main foliation with top-SE kinematics in the upper nappe: muscovite-rich Eidvågeid paragneiss

The sample is characterized by a coarse-grained (100 μm) mylonitic matrix with large (up to mm-sized) Wm fish and Grt porphyroclasts/-blasts. The mineral paragenesis consists of Qtz + Pl + Bt + Wm + Grt ± epidote (Ep) (Fig. 6f). Recrystallized Pl in the matrix has a homogeneous composition (X_{Ab} = 0.69-0.75). Bt Mg# ranges between 0.38 and 0.42. Wm occurs as mm-size Wm fish or dispersed in the foliation, where it locally forms intergrowths with Bt (Fig. 6g). Wm shows a continuum spread in composition in the range Si = 6.09-6.34 a.p.f.u.and Mg# = 0.50-0.60 (Fig. 10e) with Wm fish compositions showing lower Si and Mg# (Si = 6.09-6.14 a.p.f.u. and Mg# = 0.50-0.53). Grt shows a core-rim zoned texture: (i) the core is rich of fine-grained Qtz inclusions, (ii) the inclusion-free rim displays euhedral facets. However, the composition of Grt is fairly homogeneous from core to rim (Alm_{59-65} Grs_{23-30} Prp_{6-7}; Mg# = 0.09-0.10).

The P-T pseudosection has been calculated at H_2O-saturated conditions, as results from preliminary T-M_{H2O} pseudosection calculations (not reported here) have shown that the H_2O content derived from LOI measurements is larger than the amount of H_2O required to saturate the system. The assemblage Qtz + Bt + Pl + Grt + Wm + H_2O is stable over a wide range of P-T conditions between 550°C and 750°C and < 0.4 – 1.2 GPa. Bt Mg#, Pl X_{Ab}, Wm isopleths for Mg# and Si and Grt composition constrain the deformation conditions at 600-650°C and 0.8-0.9 GPa (Fig. 7e-f).

5.4. Main foliation with top-SE kinematics in amphibolites from the lower nappe

Sample 372 has a mylonitic fabric defined by alternating bands of amphibolite and metapelite. The amphibolite paragenesis consists of amphibole (Amp) + Pl + Bt + Ttn + Ep + Grt + Qtz ± Cpx (Fig. 8b). Cpx is mainly observed as rare relict phase. Grt + Bt + Ep paragenesis is mainly observed along amphibolite selvages in contact with metapelitic layers (Fig. 8b). Two generations of Amp have been identified based on different compositions and textures. Coarse Amp_1 porphyroclasts show a fairly homogeneous composition (Mg-hornblende; Si=6.85-7.01 a.p.f.u.; Mg#=0.68-0.7; low Al_2O_3 content). Amp_1 porphyroclasts are mantled by Amp_2 grains with lower Si and Mg# (K-Fe-pargasitic hornblende; Si=6.2-6.4; Mg#=0.58-0.61; high Al_2O_3

content). Recrystallized Pl_2 has a homogeneous composition of X_{Ab}=0.65. A few grains, possibly belonging to a former generation of Pl_1, have a slightly An-richer composition of X_{Ab}=0.57. Pl_1 and Pl_2 grains do not show any systematic textural relationship, and they are both occurring in the fine-grained amphibolite matrix. Amp-Pl geothermobarometry calculated on $Amph_2$-Pl_2 pairs yields T= 670°C ± 20 °C and P=0.98 GPa ± 0.04 GPa (Table 3).

Sample 367 is an amphibolite from tight- to isoclinal shear-parallel folds with top-to-SE sense of shear in southern Kvaløya (Fig. 3c). The mineral paragenesis consists of Amp (Si= 6.31-6.53 a.p.f.u.; Mg#= 0.57-0.63) + Pl (X_{Ab}=0.81-0.88) + Qtz + Ep + Ttn ± Rt (Fig. 8d-e). BSE images indicate that Amp is rather homogeneous in composition and does not show any core-rim zoning (Fig. 8e). Pl usually shows darker rims along grain boundaries, fractures and cleavage planes, characterized by porous aggregates of Ab-rich plagioclase (Pl_2, X_{Ab}=0.95) + Kfs + Chl (Fig. 8f). Coarse Ep shows a zoning pattern, with Fe-rich cores. Amp – Pl geothermobarometry applied to Amp – Pl mineral pairs yields consistent P-T conditions of metamorphic re-equilibration at T=650°C ± 30°C and 0.77 GPa ± 0.07 GPa.

6. $^{40}Ar/^{39}Ar$ Ages

In-situ UV Laser $^{40}Ar/^{39}Ar$ geochronological measurements were carried out on synkinematic micas on samples of: (1) the mylonitic Eidvågeid migmatite (S_m foliation in the upper nappe, sample 240) (Figs. 4b, 6c, SM2a), and (2) the muscovite-rich Eidvågeid paragneiss (main foliation with Caledonian top-to-SE kinematics in the upper nappe, sample 251) (Figs. 4e, 6f, SM2b-d). In particular, synkinematic Bt was analysed in sample 240; whereas, Bt and Wm were analysed in sample 251. The results are shown in the form of frequency diagrams in Fig. 9a-c and Table 4. The geochronology work was limited to samples of the Eidvågeid series, because the very similar bulk XRF composition between samples 240 and 251 suggests that the muscovite-rich paragneisses represent the retrograded and hydrated variety of the mylonitic Eidvågeid gneiss. Thus, we attempted to track the timing and P-T conditions of the Caledonian overprint on the Neoproterozoic fabric in samples that we considered representative of originally the same lithological unit.

6.1. Sample 240 - mylonitic Eidvågeid migmatitic gneiss

^{40}Ar/^{39}Ar data were collected in-situ from Bt aggregates in strain shadows around garnet porphyroblasts. Biotite shows no significant chemical variation (Fig. 9f). The resulting dates, as shown in the frequency distribution diagram of Fig. 9a, show a rather narrow peak resembling a (left-skewed) normal distribution centred at 423.9 ± 6.5 Ma. The dates range between 551 ± 50 Ma and 372 ± 24 Ma. No relationship between date and biotite microstructure was observed.

6.2. Sample 251 - muscovite-rich Eidvågeid paragneiss

^{40}Ar/^{39}Ar data were collected in-situ from Bt and Wm in two different textural positions: (i) fine-grained Wm (<mm-sized) lamellae in the recrystallized matrix, where muscovite is commonly intergrown with Bt (Fig. 6g); (ii) large (mm-sized) Wm fish. The chemical composition of Wm in the two different textural positions is rather different (Fig. 9e). A frequency distribution diagram shows a large spread in dates, ranging from 915 ± 87 Ma to 437 ± 10 Ma, and several scattered peaks (Fig. 9b-c). Fine-grained Bt mats yield the oldest dates (900-800 Ma). Dates between 800-500 Ma were obtained from small grains in the recrystallized matrix and from Wm grains intergrown with Bt. A population of consistently younger dates, showing a well-defined frequency peak around 489 Ma (Fig. 9c), was yielded by coarser Wm lamellae and small ‘fish’ parallel to the main mylonitic foliation.

7. Discussion

7.1. Structural and metamorphic evolution of the lower and upper nappe

Our structural analysis confirms that the lower- and upper nappe of the KNC underwent two different sequences of deformation and metamorphic events, resulting in the formation of different pre-Caledonian fabrics that were overprinted during the Caledonian continental collision (Fig. 5a). In the following discussion, we present our interpretation of the structural and metamorphic evolution of the two nappes prior and during the Caledonian orogeny.

7.1.1. Pre-Caledonian deformation in the lower nappe

Analysis of sample 360 indicates that the main gneissic banding in the Fagervik complex developed at 500-550°C and 0.7 GPa. As there is no evidence of a dextral fabric in the upper nappe, we consider the dextral fabric in the lower nappe older than 710 Ma (minimum age of the juxtaposition between lower- and upper nappe, Kirkland et al., 2006a). An earlier, higher T fabric is locally preserved as relict grains of Kfs and Sill.

The main gneissic banding has then been folded by upright folds without the development of an associated axial plane foliation. The different orientation of upright folds in northern- and southern Kvaløya suggests that upright folding was probably followed by a regional-scale bending of the fabric, and we speculate that this might have occurred during an orocline formation event (Fig. 5a) (see section 7.3.1).

The tectonometamorphic history of the lower nappe units has not been addressed in detail so far, although geochronology constraints are abundant (Kirkland et al., 2007a, 2007b). Given the lack of metamorphic constraints on the development of upright folds and the discontinuous exposure of the lower nappe between northern and southern Kvaløya, attributing the upright folding event either to pre-Caledonian discrete deformation phases or to progressive deformation in a complex regional strain field is rather difficult (Fossen et al., 2019).

This bent structural grain has been sheared during top-to-SE Caledonian thrusting, developing a heterogeneous NW-dipping foliation and different folding geometries in the northern and southern Kvaløya sections of the lower nappe.

7.1.2. Pre-Caledonian deformation in the upper nappe

The stromatic migmatite layering S_{mig} has been sheared and folded during the development of the coaxial shear zone pattern. The S_m foliation with *orogen-parallel* stretching lineation in the mylonitic Eidvågeid migmatites developed at 725-750°C, 0.65-0.8 GPa, H_2O-poor (<0.5 wt%) and melt-present conditions (Figs. 7c-d). Microstructures indicative of the former presence of melt during deformation are the Kfs films around Grt porphyroclasts and completely enveloping Pl grains (Fig. 6e, see also Menegon et al., 2011). We interpret these P-T estimates to be representative also of the conditions of S_{mig} formation in the Eidvågeid Series, as the mineral assemblages in S_{mig} and S_m are the same. Similar fabrics and microstructures indicative of high-grade, melt-present deformation in the upper nappe have been reported from many other localities of the KNC and related to the ca. 710 Ma Snøfjord event (Akkarfjord in Kvaløya: Corfu et al., 2007; Snøfjord: Kirkland et al., 2006a; Eidet: Gasser et al., 2015), indicating a pre-Caledonian age for the migmatization and mylonitization events and related structures accommodating an overall NE-SW lengthening in the lower crust. Despite the similar orientation of pre-Caledonian lineations in the upper- and in the lower nappe (subhorizontal, NE-SW, Fig. 1d), they are associated with different P-T conditions and with different deformation kinematics (Fig. 10c). This is consistent with the available geochronological constraints that indicate that the two nappes experienced different pre-

Caledonian tectono-metamorphic histories (Kirkland et al., 2005, 2007a, 2007b, 2008b; Corfu et al., 2007, 2011).

7.1.3. Caledonian evolution of the KNC

The main foliation in the lower nappe is kinematically compatible with the mylonitic foliation in the upper nappe observed at the contact zone, both showing top-to-SE kinematics. In the upper nappe, top-to-SE shearing related to Caledonian thrusting was localized exclusively in muscovite-rich Eidvågeid paragneisses. Thus, most of the upper nappe escaped the Caledonian tectonometamorphic overprint. The main foliation in muscovite-rich Eidvågeid paragneisses developed at amphibolite-facies conditions of 550-675°C, 0.8-1.0 GPa. These conditions largely overlap with the results of Amp-Pl geothermobarometry on the main mylonitic fabric developed in the lower nappe (sample 372: 650-700°C, 0.9-1.0 GPa; sample 367: 625-675°C and 0.7-0.8 GPa) (Fig. 10c). Gasser et al. (2015) obtained comparable metamorphic conditions (ca. 600-700°C, 1.0-1.2 GPa) from pseudosection analysis of the top-to-SE Caledonian fabric developed in muscovite-rich paragneisses of the KNC at the Eidet locality (Figs. 1a, 10c), which was tentatively correlated with the Eidvågeid Series. At the Eidet locality, this tectonometamorphic event has been dated at 440-430 Ma by U-Pb dating of syn-kinematic titanite (Gasser et al., 2015) and has been related to the Scandian nappe thrusting stage. As also reported by Gasser et al. (2015), the enrichment in grossular in the Grt rim compositions of the pre-Caledonian fabric in metapelitic rocks from the lower nappe is consistent with a pressure increase during Scandian overprint of the pre-Caledonian fabric (Fig. 7c-d). U-Pb titanite ages of 428.1 ± 1.6 Ma were obtained also from a Grt-Bt amphibolite the SCZ just north of Grotnes in Kvaløya (Corfu et al.,2011), the same locality of our sample 372 from the banded gneiss unit of the lower nappe , in which the main Caledonian foliation developed at 650-700°C and

0.9-1.0 GPa. Thus, we interpret the development of the main NW-dipping foliation in the lower- and upper nappes to represent the Scandian overprint during Caledonian thrusting of the KNC at P of 0.7-1.0 GPa and T of 600-700°C (Figs. 5, 10b-c).

The similarities of XRF bulk compositions and pseudosections between samples 240 and 251 suggest that the muscovite-rich Eidvågeid paragneisses might represent the product of retrogression and hydration of the Eidvågeid migmatites, which deformed under relatively dry conditions during the pre-Caledonian melt-present deformation. Comparing the pseudosection results from sample 240 (Pre-Caledonian S_m fabric in upper nappe) and sample 251 (Caledonian fabric in the upper nappe), we can infer that deformation during Caledonian overprint occurred at H_2O-saturated conditions, therefore probably involving fluid-infiltration in the upper nappe units along inherited pre-collisional tectonic nappe boundaries. Fluid infiltration along tectonic boundaries during Caledonian nappe stacking and metamorphism in the KNC has been suggested by Kirkland et al. (2009) for the explanation of zircon and monazite growth stages in the Hjelmsøy shear zone, and by Gasser et al. (2015) to account for the increased amount of Wm in the Caledonian fabric compared to the pre-Caledonian one in the Sørøy succession.

7.2. Effects of Caledonian metamorphism on $^{40}Ar/^{39}Ar$ ages

The mineral paragenesis in sample 240 equilibrated at high-grade (T > 700 °C), dry (H_2O-undersaturated) metamorphic conditions in the Neoproterozoic (maximum age of ca. 710 Ma as obtained from U-Pb zircon dating, Corfu et al., 2007; Kirkland et al., 2008b). This age and metamorphic conditions likely represent the crystallization event of the dated biotite grains. The Eidvågeid Series subsequently resided at high-T, lower crustal conditions for at least 200 Ma prior to the Caledonian orogeny (Gasser et al., 2015). Such long-lasting high-T conditions are theoretically sufficient to completely reset the isotopic system in biotite in an open system where a sink such as a grain boundary fluid is available for the released argon (Skipton et al., 2018). We therefore interpret the $^{40}Ar/^{39}Ar$ date of 423.9 ± 6.5 Ma obtained from the mylonitic Eidvågeid sample 240 as relating to the timing of cooling during the late stages of the Celdonian orogeny. This age is comparable within analytical uncertainty with other in-situ $^{40}Ar/^{39}Ar$ laser ablation biotite ages determined from paragneisses in the basement units of the Kalak and Magerøy Nappes in Finnmark (Kirkland et al., 2007a). However, we cannot exclude the possibility that contamination from excess radiogenic ^{40}Ar affected sample 240 to some degree during its tectonometamorphic (Caledonian?) history, with the effect of making the yielded date artificially too old (as also discussed by Kirkland et al., 2008a).

The development of the Caledonian fabric in muscovite-rich Eidvågeid paragneisses occurred under amphibolite facies conditions (T>550°C), at temperatures high enough to completely reset the isotopic system of Ar both in Wm and Bt at these pressures (Harrison et al., 2009; Warren et al., 2012). Importantly, Caledonian metamorphic re-equilibration involved significant fluid influx and hydration of previously dry granulitic rocks. Broad ranges of Wm and Bt $^{40}Ar/^{39}Ar$ ages have also been reported from other localities in the KNC on Sværholthalvøya and Nordkinnhalvøya ($^{40}Ar/^{39}Ar$ laser ablation geochronology; Kirkland et al., 2008a). In that study, a narrow frequency peak of Wm dates occurring around 500 Ma was interpreted by Kirkland et al. (2008a) as a Wm cooling age after a Mid-Late Cambrian tectonometamorphic event. The occurrence of older Bt ages was explained as likely due to contamination from excess radiogenic Ar in Bt from metamorphic fluids. Accordingly, similar conclusions can be drawn considering the broad date ranges reported here. Small Bt and Wm grains might have been contaminated by excess ^{40}Ar, likely related to metamorphic fluids, whereas at least the cores of the larger grains appear not to have been (Warren et al., 2012). This contamination may have occurred at relatively low temperatures (400 – 450°C), or during a short lived infiltration event: at such temperatures, the Ar isotopic system in Wm is less sensitive to contamination than in Bt (Kirkland et al., 2008a; Warren et al., 2011; Skipton et al., 2018), leading to the very much older ages in Bt compared to Wm. The effect of such contamination seems to be proportional to the amount of metamorphic re-equilibration experienced by the nappes during Caledonian collision. Bt in sample 240 might have been affected by the same fluid-infiltration event, but in a very minor amount as compared to the effect on Bt in sample 251 (which was totally re-equilibrated at Caledonian metamorphic conditions).

Our results strengthen the hypothesis that a significant regional-scale fluid-infiltration event that resulted in micas being contaminated with excess ^{40}Ar, occurred during, or shortly after, peak Caledonian metamorphic conditions were reached in the KNC (Kirkland et al., 2008a). Further geochronological analyses using different isotopic systems are needed to determine whether the obtained dates reflect the age of some regional-scale orogenic process such as metamorphic recrystallization or cooling.

7.3 Structural inheritance in the KNC during Caledonian orogenic shortening

Two puzzling structural features of the KNC in Kvaløya are (1) the different deformation style and fold orientation in the lower nappe in northern- and southern Kvaløya (Figs. 2a, 3d, 5, 10), and (2) the abrupt change in orientation of the pre-Caledonian linear fabrics , from subhorizontal NE-SW trending (*orogen-parallel*) to shallowly NW-plunging (*orogen-perpendicular*) (Fig. 1b, d). Here, we interpret both features to result from the pre-Caledonian bending of the gneissic banding in the lower nappe of the KNC.

7.3.1. Structural inheritance and the origin of orogen-parallel and orogen-perpendicular lineations

Different tectonic models have been proposed to explain a similar switch in orientation of the stretching lineation observed elsewhere in the KNC, and underlying (Laksefjord) and overlying (Magerøy) nappes. Models involve either oblique tectonics during late-stage Caledonian collision (Kirkland et al., 2006b), or shearing-related rotation of pre-existing linear fabrics (Rhodes and Gayer, 1977; Williams, 1978; Rice, 1984, 1998). The bending is most evident comparing the orientation of stretching lineations and fold axes in northern Kvaløya and in low-strain domains in southern Kvaløya, where they occur in an *orogen-parallel* and in an *orogen-perpendicular* orientation, respectively (Fig. 10a-b). The change in orientation clearly affects the lower nappe, but it is unclear if (and to what extent) it also affects the upper nappe. A similar switch in orientation of linear fabrics has been already reported from other localities within the KNC, and it has been attributed to the progressive reorientation of the fold axes of pre-Caledonian folds (generally oriented N-S to NE-SW) into the thrusting direction (Ramsay and Sturt, 1973; Rhodes and Gayer, 1977; Williams, 1978; Ramsay, 1979; Rice, 1984, 1987, 1998; Gayer et al., 1985). This reorientation is most evident and localized in the hanging wall of thrust zones and close to high-strain zones in the lowermost portions of the KNC (Zwaan and Roberts, 1978; Rice, 1987, 1998; see also Xypolias and Alsop, 2014). Conversely, in Kvaløya, the change in orientation of linear fabrics is abrupt, occurring close to the SCZ, and persistent throughout the whole investigated km-scale southern section of the nappe. Gradual re-orientation would imply a spread in the orientation of fold axes preserved in different low-strain domains, which is not observed in Kvaløya. Gradual re-orientation would also imply the development of sheath-like folds (Xypolias and Alsop, 2014), which are only locally and rarely observed in high-strain zones in Kvaløya (Fig. 3b). Therefore, we attribute the abrupt switch in orientation of the lineation to a regional-scale bending of the pre-Caledonian gneissic banding that resulted in the fold axes being oriented subparallel to the Caledonian transport direction in southern Kvaløya (Figs. 1a-b, d). Thus, the Caledonian folds in southern Kvaløya initiated with hinges parallel to the transport direction, and the abrupt change in orientation from *orogen-parallel* to *orogen-perpendicular* lineation reflects a structural inheritance during top-SE shearing of a bended pre-Caledonian structural grain.

We note that regional-scale bending of the schistosity resulting in upright folds trending from ca. NW-SE to ca. NE-SW is common in large-scale outliers of Baltica basement west of the Scandinavian Caledonides in northern Norway, such as in the West Troms Basement Complex (WTBC, Bergh et al., 2010, 2014). Granitoid rocks of ca. 1800 Ma age found in the Fagervik complex (Kirkland et al., 2006, 2008) are common also in the WTBC (Corfu et al., 2003; Bergh et al, 2010). As the Fagervik complex is interpreted as a sliver of Baltic Shield (Kirkland et al., 2008b), we infer that its southeastern transport during the Caledonian nappe stacking involved the overprint of pre-collisional folds trending both parallel and perpendicular to the Caledonian orogeny, which are preserved in e.g. the exhumed Baltica basement of the WTBC.

7.3.2. Structural inheritance vs transpressive shear during thrusting of the KNC

Strain partitioning during oblique continental collision commonly results in the development of distinct lineations related to the partitioning between orogen-parallel shear and orogen-perpendicular thrusting (Dewey et al., 1998; Goscombe et al., 2005; Viola and Henderson, 2010). Generally, sinistral transpressive shear coupled to extensional deformation coeval with the latest stages of thrusting in Late Silurian – Early Devonian time has been widely recognised in the Scandinavian Caledonides (Roberts, 2003), and typically resulted in orogen-parallel folding in the footwall of regional-scale extensional detachments (Chauvet and Séranne, 1994; Krabbendam and Dewey, 1997; Fossen, 2000). N-S to NE-SW trending, roughly *orogen-parallel* mineral lineations and fold hinges have been reported from several Caledonian nappes, including the Bergsdalen nappe in southwestern Norway (Fossen, 1993), and the KNC itself (Kirkland et al., 2006b). They have been interpreted to result from WNW-directed nappe translation prior to the development of Devonian basins in SW Norway (Fossen, 1993), and from constrictional strain during Scandian lateral escape tectonics (Kirkland et al., 2006b). However, in such a transpressive tectonics scenario, the *orogen-parallel* and the *orogen-perpendicular* lineation should be broadly coeval, develop at similar P-T conditions, and be associated with a dominant strike-slip and reverse dip-slip (top-to-SE) shearing, respectively. The results of our P-T estimates indicate that the *orogen-parallel* dextral shear in the lower nappe occurred under lower conditions than the Caledonian top-to-SE deformation in the same unit (Figs. 10c). Furthermore, neither of the kinematics associated with the *orogen-parallel* stretching lineations in the KNC is consistent with a late-Caledonian sinistral transpressive event.

The syn-collisional buttressing and lateral escape model proposed by Kirkland et al. (2006b) is based on the strain analysis of metaconglomerates with a strong N-S stretching lineation from the Magerøy nappe (structurally above the KNC), and on $^{40}Ar/^{39}Ar$ dating of biotite that defines the N-S lineation. This model assumes that the development of *orogen-parallel* and *orogen-perpendicular* lineations occurred at comparable ages and metamorphic conditions in the Magerøy nappe. The KNC on Kvaløya presents orogen-parallel lineations oriented NE-SW (different from the N-S, orientation reported from the Magerøy nappe), which (1) developed at different metamorphic conditions in the lower and upper nappes (Fig. 10c), and (2) are associated with distinct kinematics (dextral in the lower nappe vs. coaxial deformation in the upper nappe). Therefore, even though the Magerøy and the KNC nappe were already stacked during the syn-collisional Scandian lateral escape (Kirkland et al., 2006b), there is no evidence in the KNC for the occurrence of such lateral escape tectonics. The lateral escape might have affected only the overlying Magerøy nappe, suggesting a sort of orogen-scale strain partitioning between nappes.

7.3.3. Structural inheritance and orogen-scale strain partitioning during Caledonian deformation

The upper and the lower units show a different tectonic style during Caledonian overprint. The upper nappe was largely unaffected by Caledonian deformation, except at its southern margin (SCZ), where muscovite-rich Eidvågeid paragneisses are optimally oriented (shallowly NW-dipping) to localise top-to-SE shearing (Fig. 4e). The Caledonian high-strain zone at the southern contact zone represents an internal thrust within the KNC (Fig. 10a-b) and exploits the terrane boundary between the upper and lower nappes (see also Kirkland et al., 2006b).

The hangingwall of the internal thrust (northern and central Kvaløya, Figs. 1b, 5b, 10a-b) extensively preserves pre-Caledonian *orogen-parallel* fabrics, suggesting that the intensity of the Caledonian tectonic overprint was low there. Thus, we interpret northern and central Kvaløya as a Caledonian low-strain domain. The weak Caledonian overprint in the lower nappe resulted in a tilting of the NE-SW-trending upright folds to produce slightly asymmetric SE-verging folds. Caledonian stretching lineations developed only on fold limbs that were progressively tilted from subvertical to NW-dipping, and then optimally oriented for top-to-SE shear localization (Akselsen, 1982). In central Kvaløya, the upper nappe behaved as an orogen-scale “porphyroclast” during Caledonian deformation. This behaviour is typical of lower crustal, dry, granulitic terranes that can survive metastably during the Wilson cycle if they are not infiltrated by aqueous fluids and weakened (Yardley and Valley, 1997; Austrheim, 2013). Indeed, fluid-infiltration, metamorphic re-equilibration and weakening probably occurred at the boundary between upper- and lower nappe, developing the muscovite-rich Eidvågeid paragneisses, on which Caledonian shearing had preferentially localized.

The Caledonian overprint was more pervasive in the footwall of the internal thrust, towards the foreland. In southern Kvaløya, the pre-Caledonian fabric in the lower nappe was not suitably oriented to localize Caledonian shearing, given that axes of upright folds were parallel to the top-to-SE tectonic transport direction. Caledonian folds initiated with hinges subparallel to the stretching lineation and evolved (Fig. 11a, c), with progressively higher strain, into the development of recumbent folds with a new, Caledonian axial planar foliation with top-to-SE kinematic indicators. Upright folds were progressively vertically flattened with strain (Fig. 11b, d). Flattening and hinge-parallel shearing lead to the development of “curtain folds” (Xypolias et al., 2013) and Type-3 re-folded structures (Grasemann et al., 2004) that progressively evolved into recumbent folds with a shallowly NW-dipping axial plane (Fig. 11e-f). Thus, the pervasive Caledonian foliation in the lower nappe in southern Kvaløya developed as an axial plane foliation from the transposition of previous upright folds. This evolution of fold geometry highlights the strong strain partitioning between the low-strain domains, where pure-shear component is mainly partitioned, and the enveloping Caledonian S_3 foliation, where the top-to-SE simple-shear component is accommodated (Fig. 11g).

8. Conclusions

This study highlights the pivotal role of integrated field, microstructural, petrological and geochronological analysis in untangling the tectonometamorphic history of polyorogenic nappe systems. Geochronological and petrological analysis are fundamental for discerning between pre- and/or syn-collisional fabrics and structures with similar orientation, which might otherwise be related to a common tectonometamorphic event. For example, in the KNC there is evidence for at least three different deformation events (two pre-Caledonian and one Caledonian) associated with orogen-parallel stretching lineations.

The definition of the tectonometamorphic history and related fabrics in the KNC has clarified how pre-collisional fabrics controlled strain partitioning during Caledonian shortening. The structural character (massive vs layered) and the metamorphic history of the pre-collisional fabrics strongly influenced partitioning of both strain intensity and geometry during Caledonian shortening. The top-to-SE thrusting component of Caledonian general shear was initially partitioned onto inherited, optimally-oriented pre-collisional tectonic boundaries between the upper and lower nappe. These structures were hydrated and weakened during Caledonian shortening and metamorphic re-equilibration. Strain intensity increased towards the south east with the development of suitably-oriented fabric during initially flattening-dominated general shear of the lower nappe in southern Kvaløya.

Fluid-related contamination of excess ^{40}Ar appears to have influenced the dates recorded in synkinematic micas of the Caledonian fabric. Our results and those available in the literature suggest that Arctic Caledonides $^{40}Ar/^{39}Ar$ mica dates should be carefully interpreted in relation with their Caledonian metamorphic evolution, since fluid-related radiogenic Ar contamination appears widespread. We suggest that our approach provides a suitable framework for disentangling the complex poly-orogenic tectonometamorphic evolution of lower crustal nappes in the Caledonides and elsewhere. However, further studies involving different geochronological methods are needed to provide more robust temporal constraints.

Acknowledgments

This study was funded by a FP7 Marie Curie Career Integration Grant to LM (grant agreement PCIG13-GA-2013-618289). We thank Holger Stünitz, Petr Jeřábek, Deta Gasser, Hugh Rice, Åke Fagereng, and Nadia Malaspina for many fruitful discussions in the course of this work. The staff at the electron microprobe laboratory at the University of Vienna and at the University of Plymouth Electronic Microscopy Centre are thanked for their support during the analysis. Giulia degli Alessandrini is thanked for her support during EMPA analysis at the Open University. Our new geological mapping has drawn on the undergraduate projects of Jamie Lott, Alex Kelly, James Forbes and Sebastian Hind at the University of Plymouth. We gratefully acknowledge the thorough and constructive reviews by Haakon Fossen and Chris Kirkland, and the invaluable editorial handling by Stephen Laubach.

References

Akselsen, J., 1982. Precambrian and Caledonian tectonometamorphic evolution of northeastern Seiland, Finnmark, North Norway. Nor. Geol. Unders. Bull, 373, 45-61.

Audet, P., and Bürgmann, R., 2011. Dominant role of tectonic inheritance in supercontinent cycles. Nature Geoscience, 4(3), 184-187.

Austrheim, H., 2013. Fluid and deformation induced metamorphic processes around Moho beneath continent collision zones: Examples from the exposed root zone of the Caledonian mountain belt, W-Norway. Tectonophysics, 609, 620-635.

Babist, J., Handy, M. R., Konrad-Schmolke, M., Hammerschmidt, K., 2006. Precollisional, multistage exhumation of subducted continental crust: The Sesia Zone, western Alps. Tectonics, 25(6).

Bastida, F., Aller, J., Fernandez, F. J., Lisle, R. J., Bobillo-Ares, N. C., Menendez, O., 2014. Recumbent folds: key structural elements in orogenic belts. Earth-science reviews, 135, 162-183.

Beaumont, C., Nguyen, M. H., Jamieson, R. A., Ellis, S., 2006. Crustal flow modes in large hot orogens. Geological Society, London, Special Publications, 268(1), 91-145.

Beltrando, M., Manatschal, G., Mohn, G., Dal Piaz, G. V., Brovarone, A. V., Masini, E., 2014. Recognizing remnants of magma-poor rifted margins in high-pressure orogenic belts: The Alpine case study. Earth-Science Reviews, 131, 88-115.

Bergh, S. G., Kullerud, K., Myhre, P. I., Corfu, F., Armitage, P. E. B., Zwaan, K. B., Ravna, E. J. K., 2014. Archaean elements of the basement outliers west of the Scandinavian Caledonides in Northern Norway: architecture, evolution and possible correlation with

Fennoscandia. In Evolution of Archean Crust and Early Life (pp. 103-126). Springer, Dordrecht.

Bhadra, S., and Bhattacharya, A., 2007. The barometer tremolite+ tschermakite+ 2 albite= 2 pargasite+ 8 quartz: Constraints from experimental data at unit silica activity, with application to garnet-free natural assemblages. American Mineralogist, 92(4), 491-502.

Butler, R. W., Tavarnelli, E., Grasso, M., 2006. Structural inheritance in mountain belts: an Alpine–Apennine perspective. Journal of Structural Geology, 28(11), 1893-1908.

Chauvet, A., and Séranne, M., 1994. Extension-parallel folding in the Scandinavian Caledonides: implications for late-orogenic processes. Tectonophysics, 238(1-4), 31-54.

Connolly, J. A., 2005. Computation of phase equilibria by linear programming: a tool for geodynamic modeling and its application to subduction zone decarbonation. Earth and Planetary Science Letters 236, 524-541.

Corfu, F., Armitage, P.E.B., Kullerud, K., Bergh, S.G., 2003: Preliminary U-Pb geochronology in the West Troms Basement Complex, North Norway: Archaean and Palaeoproterozoic events and younger overprints. Norges geologiske undersøkelse Bulletin 441, 61-72

Corfu, F., Roberts, R. J., Torsvik, T. H., Ashwal, L. D., Ramsay, D. M., 2007. Peri-Gondwanan elements in the Caledonian Nappes of Finnmark, Northern Norway: Implications for the paleogeographic framework of the Scandinavian Caledonides. American Journal of Science, 307, 434-458.

Corfu, F., Gerber, M., Andersen, T. B., Torsvik, T. H., Ashwal, L. D., 2011. Age and significance of Grenvillian and Silurian orogenic events in the Finnmarkian Caledonides, northern Norway. Canadian Journal of Earth Sciences, 48, 419-440.

Culshaw, N., Gerbi, C., Marsh, J., 2010. Softening the lower crust: Modes of syn-transport transposition around and adjacent to a deep crustal granulite nappe, Parry Sound domain, Grenville Province, Ontario, Canada. Tectonics, 29(5).

Daly, J. S., Aitcheson, S. J., Cliff, R. A., Gayer, R. A., Rice, A. H. N., 1991. Geochronological evidence from discordant plutons for a late Proterozoic orogen in the Caledonides of Finnmark, northern Norway. Journal of the Geological Society, 148, 29-40.

Dewey, J. F., Holdsworth, R. E., Strachan, R. A., 1998. Transpression and transtension zones. Geological Society, London, Special Publications, 135(1), 1-14.

Elvevold, S., Reginiussen, H., Krogh, E. J., Bjørklund, F., 1994. Reworking of deep-seated gabbros and associated contact metamorphosed paragneisses in the southeastern part of the Seiland Igneous Province, northern Norway. Journal of Metamorphic Geology, 12(4), 539-556.

Escher, A., and Beaumont, C., 1997. Formation, burial and exhumation of basement nappes at crustal scale: a geometric model based on the Western Swiss-Italian Alps. Journal of Structural geology, 19(7), 955-974.

Faber, C., Stünitz, H., Gasser, D., Jeřábek, P., Kraus, K., Corfu, F., Ravna, E. K., Konopásek, J., 2019. An anticlockwise metamorphic P-T path and nappe stacking in the Reisa Nappe Complex in the Scandinavian Caledonides, northern Norway: evidence for weakening of lower continental crust before and during continental collision. Solid Earth, 10, 117–148, 2019, https://doi.org/10.5194/se-10-117-2019

Fossen, H., 1993. Linear fabrics in the Bergsdalen Nappes, southwest Norway: implications for deformation history and fold development. Norsk Geologisk Tidsskrift, 73(2), 95-108.

Fossen, H., 2000. Extensional tectonics in the Caledonides: Synorogenic or postorogenic?. Tectonics, 19(2), 213-224.

Fossen, H., and Cavalcante, G. C. G., 2017. Shear zones–A review. Earth-Science Reviews, 171, 434-455.

Fossen, H., Khani, H. F., Faleide, J. I., Ksienzyk, A. K., Dunlap, W. J., 2017. Post-Caledonian extension in the West Norway–northern North Sea region: the role of structural inheritance. Geological Society, London, Special Publications, 439(1), 465-486.

Fossen, H., Cavalcante, G. C. G., Pinheiro, R. V. L., Archanjo, C. J., 2019. Deformation–progressive or multiphase?. Journal of Structural Geology, 125, 82-99.Gayer, R. A., Hayes, S. J., Rice, A. H. N., 1985. The structural development of the Kalak Nappe Complex of eastern and central Porsangerhalvøya, Finnmark, Norway. Universitetsforlaget.

Gasser, D., Jeřábek, P., Faber, C., Stünitz, H., Menegon, L., Corfu, F., Whitehouse, M. J., 2015. Behaviour of geochronometers and timing of metamorphic reactions during deformation at lower crustal conditions: phase equilibrium modelling and U–Pb dating of zircon, monazite, rutile and titanite from the Kalak Nappe Complex, northern Norway. Journal of metamorphic Geology, 33, 513-534.

Gee, D. G., Fossen, H., Henriksen, N., Higgins, A. K., 2008. From the early Paleozoic platforms of Baltica and Laurentia to the Caledonide Orogen of Scandinavia and Greenland. Episodes, 31(1), 44-51.

Gee, D. G., Andréasson, P. G., Li, Y., Krill, A., 2017. Baltoscandian margin, Sveconorwegian crust lost by subduction during Caledonian collisional orogeny. GFF, 139(1), 36-51.

Goscombe, B., Gray, D., Hand, M., 2005. Extrusional tectonics in the core of a transpressional orogen; the Kaoko Belt, Namibia. Journal of Petrology, 46(6), 1203-1241.

Grasemann, B., Wiesmayr, G., Draganits, E., Fusseis, F., 2004. Classification of refold structures. The Journal of geology, 112(1), 119-125.

Harrison, T.M., Célérier, J., Aikman, A.B., Hermann, J., Heizler, M.T., 2009. Diffusion of 40Ar in muscovite. Geochimica et Cosmochimica Acta, 73(4), pp.1039-1051.

Holland, T., and Blundy, J., 1994. Non-ideal interactions in calcic amphiboles and their bearing on amphibole-plagioclase thermometry. Contributions to mineralogy and petrology, 116(4), 433-447.

Holland, T. J. B., and Powell, R., 2011. An improved and extended internally consistent thermodynamic dataset for phases of petrological interest, involving a new equation of state for solids. Journal of Metamorphic Geology 29, 333-383.

Jammes, S., and Huismans, R. S., 2012. Structural styles of mountain building: Controls of lithospheric rheologic stratification and extensional inheritance. Journal of Geophysical Research: Solid Earth, 117(B10).

Jansen, Ø, Akselsen, J., Roberts, D., 2012: Berggrunnsgeologisk kart HAMMERFEST 1936 III, M 1:50 000, foreløpig utgave. Norsk geologiske undersøkelse.

Kirkland, C. L., Daly, J. S., Whitehouse, M. J., 2005. Early Silurian magmatism and the Scandian evolution of the Kalak nappe complex, Finnmark, Arctic Norway. Journal of the Geological Society, 162(6), 985-1003.

Kirkland, C. L., Daly, J. S., Whitehouse, M. J., 2006a. Granitic magmatism of Grenvillian and late Neoproterozoic age in Finnmark, Arctic Norway—constraining pre-Scandian deformation in the Kalak Nappe Complex. Precambrian Research, 145, 24-52.

Kirkland, C. L., Daly, J. S., Eide, E. A., Whitehouse, M. J., 2006b. The structure and timing of lateral escape during the Scandian Orogeny: a combined strain and geochronological investigation in Finnmark, Arctic Norwegian Caledonides. Tectonophysics, 425(1-4), 159-189.

Kirkland, C. L., Daly, J. S., Eide, E. A., Whitehouse, M. J., 2007a. Tectonic evolution of the Arctic Norwegian Caledonides from a texturally-and structurally-constrained multi-isotopic (Ar-Ar, Rb-Sr, Sm-Nd, U-Pb) study. American Journal of Science, 307, 459-526.

Kirkland, C. L., Stephen Daly, J., Whitehouse, M. J., 2007b. Provenance and terrane evolution of the Kalak Nappe Complex, Norwegian Caledonides: implications for Neoproterozoic paleogeography and tectonics. The Journal of Geology, 115, 21-41.

Kirkland, C. L., Daly, J. S., Chew, D. M., Page, L. M., 2008a. The Finnmarkian Orogeny revisited: an isotopic investigation in eastern Finnmark, Arctic Norway. Tectonophysics, 460, 158-177.

Kirkland, C. L., Daly, J. S., Whitehouse, M. J., 2008b. Basement–cover relationships of the Kalak Nappe Complex, Arctic Norwegian Caledonides and constraints on Neoproterozoic terrane assembly in the North Atlantic region. Precambrian Research, 160, 245-276.

Kirkland, C. L., Whitehouse, M. J., Slagstad, T., 2009. Fluid-assisted zircon and monazite growth within a shear zone: a case study from Finnmark, Arctic Norway. Contributions to Mineralogy and Petrology, 158, 637-657.

Kirkland, C. L., Erickson, T. M., Johnson, T. E., Danišík, M., Evans, N. J., Bourdet, J., McDonald, B. J., 2016. Discriminating prolonged, episodic or disturbed monazite age spectra: An example from the Kalak Nappe Complex, Arctic Norway. Chemical Geology, 424, 96-110.

Krabbendam, M., and Dewey, J. F., 1998. Exhumation of UHP rocks by transtension in the Western Gneiss Region, Scandinavian Caledonides. Geological Society, London, Special Publications, 135(1), 159-181.

Manzotti, P., and Zucali, M., 2012. The pre-Alpine tectonic history of the Austroalpine continental basement in the Valpelline unit (Western Italian Alps). Geological Magazine, 150(1), 153-172.

Massironi, M., Bistacchi, A., Menegon, L., 2011. Misoriented faults in exhumed metamorphic complexes: rule or exception?. Earth and Planetary Science Letters, 307(1-2), 233-239.

Mouthereau, F., Watts, A. B., Burov, E., 2013. Structure of orogenic belts controlled by lithosphere age. Nature geoscience, 6(9), 785.

Ramsay, J. G., 1962. Interference patterns produced by the superposition of folds of similar type. The Journal of Geology, 70(4), 466-481.

Ramsay, D. M., 1979. Analysis of rotation of folds during progressive deformation. Geological Society of America Bulletin, 90(8), 732-738.

Ramsay, D. M., and Sturt, B. A., 1973. An analysis of noncylindrical and incongruous fold pattern from the eo-cambrian rocks of Sørøy, northern Norway: I. Noncylindrical, incongruous and aberrant folding. Tectonophysics, 18(1-2), 81-107.

Ramsay, D. M., Sturt, B. A., Jansen, Ø., Andersen, T. B., Sinha-Roy, S., 1985. The tectonostratigraphy of western Porsangerhalvøya, Finnmark, north Norway. The Caledonide

Orogen: Scandinavia and related areas. Edited by DG Gee and BA Sturt. John Wiley, Chichester, UK, 611-619.

Renne, P. R., Balco, G., Ludwig, K. R., Mundil, R., Min, K., 2011. Response to the comment by WH Schwarz et al. on “Joint determination of 40K decay constants and 40Ar∗/40K for the Fish Canyon sanidine standard, and improved accuracy for 40Ar/39Ar geochronology” by PR Renne et al.(2010). Geochimica et Cosmochimica Acta, 75(17), 5097-5100.

Rhodes, S., and Gayer, R. A., 1977. Non-cylindrical folds, linear structures in the X direction and mylonite developed during translation of the Caledonian Kalak nappe complex of Finnmark. Geological Magazine, 114, 329-341.

Rice, A. H. N., 1984. The significance of a thrust fault lineation in the Kalak Nappe Complex of Finnmark. Norsk geologisk tidsskrift, 64, 173-180.

Rice, A. H. N., 1987. Continuous out-of-sequence ductile thrusting in the Norwegian Caledonides. Geological Magazine, 124(3), 249-260.

Rice, A. H. N., 1990. Possible basement rocks in the Kalak Nappe Complex on Sørøy, Finnmark, N. Norway. Norsk Geologisk Tidsskrift, 70, 159-172.

Rice, A. H. N., 1998. Stretching lineations and structural evolution of the Kalak Nappe Complex (Middle Allochthon) in the Repparfjord-Fægfjord area, Finnmark, northern Norway. Norsk Geologisk Tidsskrift, 78, 277-289.

Rice, A. H. N., and Frank, W., 2003. The early Caledonian (Finnmarkian) event reassessed in Finnmark: 40Ar/39Ar cleavage age data from NW Varangerhalvøya, N. Norway. Tectonophysics, 374(3-4), 219-236.

Rice, A. H. N., and Roberts, D., 1988. Multi-textured garnets from a single growth event: an example from northern Norway. Journal of Metamorphic Geology, 6(2), 159-172.

Ridley, J., 1989. Structural and metamorphic history of a segment of the Sesia-Lanzo zone, and its bearing on the kinematics of Alpine deformation in the western Alps. Geological Society, London, Special Publications, 45(1), 189-201.

Roberts, D., 2003. The Scandinavian Caledonides: event chronology, palaeogeographic settings and likely modern analogues. Tectonophysics, 365(1-4), 283-299.

Roberts, R. J., Corfu, F., Torsvik, T. H., Ashwal, L. D., Ramsay, D. M., 2006. Short-lived mafic magmatism at 560–570 Ma in the northern Norwegian Caledonides: U–Pb zircon ages from the Seiland Igneous Province. Geological Magazine, 143, 887-903.

Skipton, D.R., Warren, C.J. Hanke, F., 2018. Numerical models of P–T, time and grain-size controls on Ar diffusion in biotite: An aide to interpreting 40Ar/39Ar ages. Chemical Geology, 496, pp.14-24.

Slagstad, T., Melezhik, V. A., Kirkland, C. L., Zwaan, K. B., Roberts, D., Gorokhov, I. M., Fallick, A. E., 2006. Carbonate isotope chemostratigraphy suggests revisions to the geological history of the West Finnmark Caledonides, northern Norway. Journal of the Geological Society, 163(2), 277-289.

Spalla, M. I., Zucali, M., Di Paola, S., Gosso, G., 2005. A critical assessment of the tectono-thermal memory of rocks and definition of tectono-metamorphic units: evidence from fabric and degree of metamorphic transformations. Geological Society, London, Special Publications, 243(1), 227-247.

Sturt, B. A., Pringle, I. R., Ramsay, D. M., 1978. The Finnmarkian phase of the Caledonian orogeny. Journal of the Geological Society, 135(6), 597-610.

Vauchez, A., and Barruol, G., 1996. Shear-wave splitting in the Appalachians and the Pyrenees: importance of the inherited tectonic fabric of the lithosphere. Physics of the earth and planetary interiors, 95(3-4), 127-138.

Viola, G., and Henderson, I. C., 2010. Inclined transpression at the toe of an arcuate thrust: an example from the Precambrian ‘Mylonite Zone’of the Sveconorwegian orogen. Geological Society, London, Special Publications, 335(1), 715-737.

Waldbaum, D. R., Thompson Jr, J. B., 1969. Mixing properties of sanidine crystalline solutions: IV. Phase diagrams from equations of state. American Mineralogist: Journal of Earth and Planetary Materials, 54, 1274-1298.

Warren, C.J., Hanke, F. Kelley, S.P., 2012. When can muscovite 40Ar/39Ar dating constrain the timing of metamorphic exhumation?. Chemical Geology, 291, pp.79-86.

Wex, S., Mancktelow, N. S., Hawemann, F., Camacho, A., Pennacchioni, G., 2017. Geometry of a large-scale, low-angle, midcrustal thrust (Woodroffe Thrust, central Australia). Tectonics, 36(11), 2447-2476.

White, R. W., Powell, R., Johnson, T. E., 2014. The effect of Mn on mineral stability in metapelites revisited: new a–x relations for manganese-bearing minerals. Journal of Metamorphic Geology, 32, 809-828.

Whitney, D. L., and Evans, B. W., 2010. Abbreviations for names of rock-forming minerals. American mineralogist, 95(1), 185-187.

Williams, G. D., 1978. Rotation of contemporary folds into the X direction during overthrust processes in Laksefjord, Finnmark. Tectonophysics, 48, 29-40.

Williams, P. F., and Jiang, D., 2005. An investigation of lower crustal deformation: Evidence for channel flow and its implications for tectonics and structural studies. Journal of Structural Geology, 27(8), 1486-1504.

Worthing, M. A., 1984. Rotated boudins associated with Caledonian thrusting from Seiland, North Norway. Norwegian Journal of Geology, 61, 70.

Xypolias, P., Chatzaras, V., Beane, R., Papadopoulou, S., 2013. Heterogeneous constrictional deformation in a ductile shear zone resulting from the transposition of a lineation-parallel fold. Journal of Structural Geology, 52, 44-59.

Xypolias, P., and Alsop, G. I., 2014. Regional flow perturbation folding within an exhumation channel: a case study from the Cycladic Blueschists. Journal of Structural Geology, 62, 141-155.

Yardley, B. W., and Valley, J. W., 1997. The petrologic case for a dry lower crust. Journal of Geophysical Research: Solid Earth, 102(B6), 12173-12185.

Zwaan, K. B. and Roberts, D. 1978: Tectonostratigraphic succession and development of the Finnmarkian nappe sequence, North Norway. Norges geol. Unders. 343, 53-71.

Figure Captions

Figure 1: Geological map and structural orientation data obtained from field survey. Geographical coordinate system WGS84. (a) Geographical location and geological map of Finnmark, northern Norway (redrawn from Gayer et al., 1987; Kirkland et al., 2007a, 2008a; Gasser et al., 2015). DTM base layer elaborated from USGS Aster GDEM database (https://earthexplorer.usgs.gov/). (b) Tectonostratigraphic column showing the interpreted units belonging to the upper and lower nappes observed in Kvaløya. The Contact Zone (faint wavy curve) is interpreted here as a tectonically re-elaborated tectonic contact. (c) Geological map of Kvaløya. The map shows also the location of analysed samples (encircled numbers from 1 to 5) and the trace of the interpreted cross section shown in Fig. 5b. (d) Equal area, lower hemisphere projection of structural orientation data from the identified structural domains and nappes exposed in Kvaløya; left column reports poles to foliation and lineations; right column reports fold axes and poles to axial plane. Dashed grey great circles represent the orientation of the mean girdle distribution of foliation calculated from lineation distribution. Black dashed great circles represent the average orientation of fold axial plane. Beta-axes and calculated average orientation of linear fabrics are reported (grey-filled squares and triangles for beta/fold-axes and lineations, respectively). Abbreviations: $\mathbf{S_G}$: gneissic banding in the lower nappe; $\mathbf{L_{SG}}$: stretching lineation of the gneissic banding; $\mathbf{L_{Smain}}$: stretching lineation of the NW-dipping main foliation; $\mathbf{S_m}$: mylonitic foliation in the upper nappe; $\mathbf{L_{Sm}}$: stretching lineation on the mylonitic foliation of the upper nappe.

Figure 2: Lower nappe structure in northern Kvaløya. (a) Symmetrical upright folds in the Fagervik banded gneisses on the northern slope of Rypefjell. Field of view: 40 m. (b) Slightly SE-vergent upright fold refolding the main geissic banding in the Fagervik gneisses. The gneissic banding is here defined by the alternation of pegmatitic gneiss layers (Pegm),

paragneisses (Para-gns) and amphibolite (Amph) layers. The hinge zone of an upright fold is exposed, showing the parallelism between crenulation L_C and stretching L_S lineations. (c) Typical outcrop of the Rusty Unit on the southern slope of Rypefjell. Note the succession of cm-thick layers of metapelites, quartzite and a thick layers with mafic composition. On the right side of the outcrop, it is possible to see the typical "rusty"-like alteration of this unit. (d) Top-to-NE (dextral) shear-sense indicator (amphibolite lense) in the banded gneiss unit. Norwegian krone coin for scale. Orientation of filed images is usually vertical, where not otherwise specified.

Figure 3: Lower nappe structure in southern Kvaløya. (a) Sheared and re-folded gneissic banding (black lines) enveloped by the NW-dipping foliation (white lines) in a pelitic facies of the banded gneiss unit close to the SCZ. (b) Sheath-like fold geometry (gneissic banding sheared and re-folded within dominant NW-dipping foliation – white lines) observed in the fine-grained mylonitic facies of the banded gneiss unit close to the SCZ. (c) Asymmetric boudinage in a competent amphibolite layer of the Fagervik gneiss complex indicating top-to-SE shearing along the main foliation (sample 367, locality 4 in Figs. 1b, 5b). (d) Overprinting fabrics in the Særholt Psammites (Southern Kvaløya). Inferred top-to-SE kinematic is shown on the main foliation. A lensoid low-strain domain, preserving at its interior the upright folds, is enveloped by shallowly NW-dipping foliation. (e) Tight shear-parallel fold in the banded gneiss unit in the "Southern Contact Zone". The tightly re-folded and flattened pre-Caledonian fabric is marked by black lines.

Figure 4: Fabrics of the Eidvågeid Paragneisses in the Upper Nappe. (a) Typical outcrop of the Eidvågeid Migmatitic facies showing the stromatic banding of melanosomes and leucosomes. (b) Mylonitic facies of Eidvågeid showing the characteristic dark pink garnets. No clear shear sense indicators are observed. (c) Crosscutting relationships between the subvertical

S_{mig} fabric (dashed white curves) of the migmatitic facies and the subhorizontal S_m (solid white lines) mylonitic facies of Eidvågeid. (d) Outcrop of the muscovite-rich Eidvågeid NW-dipping foliation overprinting the mylonitic Eidvågeid S_m fabric (location close to the SCZ). (e) Muscovite-rich Eidvågeid showing top-to-SE kinematic indicators (feldspar sigma-clast in this case).

Figure 5. (a) Annotated sketches that summarize the deformation history of the KNC in Kvaløya inferred from field observations (see text for explanation). (b) Geological cross section of Kvaløya along the profile A-A' of Fig. 1b and sample locations.

Figure 6. Petrography and microstructures of the analysed samples. (a) Optical image (crossed polarizers) of the microstructure of sample 360 – banded gneiss unit showing top-to-NE kinematics and orogen-parallel lineations. (b) Detail of the microstructure of sample 360 showing Sill porphyroclasts embedded in white Wm (optical microscope, crossed polarizers). (c) Optical image (crossed polarizers) displaying the microstructure of sample 240 – Mylonitic Eidvågeid showing the banding defined by Qtz and Qtz + Kfs + Bt layers embedding Pl porphyroclasts and Grt porphyroblasts. (d) BSE image of the microstructure of sample 240. (e) Detail of the microstructure of sample 240 showing thin Kfs layers around Pl porphyroclasts interpreted as former melt layers (BSE image). (f) Optical image (crossed polarizers) of sample 251 – muscovite-rich Eidvågeid showing Wm fish embedded in Wm + Bt foliation. (g-h) BSE image of sample 251 microstructure showing the occurrence of Pl porphyroclasts, WM fish and Wm-Bt intergrowths along the foliation.

Figure 7. P-T Phase diagram sections and summary of P-T conditions obtained from petrological analysis of other outcrop of the KNC. (a) (c) (e) P-T pseudosections for sample 360, 240, 251, respectively, showing the observed stable metamorphic assemblage and the P-T field (red polygons) refined by isopleths analysis. (b) (d) (f) P-T pseudosections for sample

360, 240, 251, respectively, showing the Mg# and XGrs isopleths adopted in each sample for the P-T conditions refinement. In each diagram are reported the most relevant mineral-in and/or -out reactions and XGrs and Mg# isopleths for garnet. In (c-d), the inferred conditions of formation of Grt rims of sample 240 and relevant X_{Ab} and Bt Mg# isopleths are reported.

Figure 8. Microstructure of amphibolite samples of the banded gneiss and Fagervik Units (a) Sample 372 – Mylonitic facies of banded gneiss unit showing asymmetric Pl porphyroclasts suggesting top-to-SE kinematics. (b) Optical microphotograph of amphibolite sample 372 from the banded gneiss unit (Sample 4 of Fig. 5). (b) SEM-BSE image of the white box reported in (b). (d) Optical microphotograph of amphibolite sample 367 from the Fagervik gneisses (Sample 5 of Fig. 5). (e) SEM-BSE image of the white box reported in (d). (f) BSE image of a detail of the microstructure of sample 367 showing the local nucleation of Ab and Chl.

Figure 9. Linear probability plot of dates resulting from Wm and Bt in-situ $^{40}Ar/^{39}Ar$ geochronology. Plotted dates have 95% confidence and are presented in ascending order from left to right. Box heights (error bars) are 2σ. Dates presented in blue bars were rejected. (a) Age spectra resulting from in situ analysis on Bt from Mylonitic Eidvågeid S_m fabric. (b) Whole age spectra resulting from in situ analysis on white Wm from muscovite-rich Eidvågeid main fabric. (c) Age spectra of the younger population obtained from in situ analysis on white Wm from muscovite-rich Eidvågeid shown in (b). (d) Age absolute frequency diagram of sample 251 compared to selected age spectra from Kirkland et al. (2008a). (e) Si vs Mg# diagram for Wm of sample 251. (f) Si vs Mg# diagram showing the composition of Bt in sample 251 and 240.

Figure 10. Block diagrams representing the pre- and collisional fabrics in the KNC. (a). Pre-collisional (post-bending) structural setting and fabrics in the KNC. The lower nappe presents the upright symmetric folds with different orientation in northern and southern Kvaløya. The

upper nappe is characterized by the migmatitic and mylonitic fabrics. (b) Structural setting and fabrics developed during the Caledonian shortening. The block diagram shows the increasing intensity of strain accommodated toward the foreland. The pre-collisional fabric in the lower nappe is tilted toward SE in northern Kvaløya; whereas it is flattened and then sheared in southern Kvaløya. The pre-collisional fabric in the upper nappe is exploited only where it is favourably oriented along the pre-collisional nappe contact (orange layers). The exploitation of such pre-collisional contact gave rise to a zone of localized shearing internal to the nappe during Caledonian shortening. (c) P-T diagram summing up the metamorphic conditions obtained from this work and compared to the P-T estimates published in the literature for other outcrops of the KNC (Gasser et al., 2015; Faber et al., 2019). Numbers in parenthesis refers to the sample (1-5) reported in this work.

Figure 11. Development of shear-parallel folds. See text for explanation.

Tables

Table 1. Bulk compositions of the rock samples as obtained from XRF analyses and adopted for pseudosection calculation .

Table 2. Mineral phase compositions of the rock samples as obtained from EMP analysis.

Table 3. Mineral phase compositions of Amp and Pl as obtained from EMP analysis on amphibolite samples 372 and 367 with the respective claculated standard deviations. Pressure and temperature results are reported as obtained from Amp-Pl geothermobarometry applied to selected Amp-Pl pairs.

Table 4. In situ UV laser ablation ^{40}Ar/^{39}Ar of synkinematic micas analysed in the Samples 240 and 251.

Table 1.

Sample	360	240	251
SiO_2	63.91	69.40	66.42
TiO_2	1.01	1.01	0.80
Al_2O_3	18.55	13.91	14.75
FeO	5.43	5.15	5.82
MnO	0.08	0.10	0.14
MgO	1.60	1.52	1.77
CaO	0.89	2.27	2.20
Na_2O	1.49	2.34	2.77
K_2O	3.91	2.80	2.83
P_2O_5	0.14	0.09	0.22
Total	97.00	98.59	97.71
LOI	1.74	0.12	0.78
SO_3	0.003	-0.004	-0.002
V_2O_5	0.018	0.015	0.015
Cr_2O_3	0.008	0.005	0.005
SrO	0.003	0.008	0.009
ZrO_2	0.038	0.064	0.035
BaO	0.094	0.112	0.076
NiO	0.003	0.003	0.002
CuO	BDL	BDL	0.003
ZnO	0.014	0.008	0.018
PbO	0.004	0.009	0.006
HfO_2	0.001	0.001	BDL

Table 2.

Unit	Lower Nappe (North) - Rusty Unit				Upper Nappe - Mylonitic Eidvågeid				Upper Nappe - Wm-bearing Eidvågeid			
Sample	1 - 360				2 - 240				3 -251			
Mineral phase	Pl	Bt	Wm	Grt	Pl	Bt	Grt (core)	Grt (rim)	Pl	Bt	Wm	Grt
Number of point analysis	8	10	14	10	18	29	8	19	16	19	50	9.00
Component												
Na_2O	9.30	0.14	0.53	0.00	7.41	0.15	0.07	0.06	8.52	0.11	0.31	0.09
MgO	0.00	9.94	1.02	3.53	-0.02	10.73	5.82	4.32	0.01	7.74	1.42	1.85
Al_2O_3	23.28	18.07	33.93	21.07	25.50	18.31	21.64	21.65	23.74	17.62	32.31	21.51
SiO2	63.12	36.12	47.56	37.59	59.39	36.38	37.76	37.62	61.95	35.92	47.79	37.43
K_2O	0.03	8.21	9.63	-0.02	0.22	9.81	0.00	0.00	0.27	9.27	10.31	0.00
CaO	4.46	0.04	-0.01	2.66	7.24	0.04	1.66	4.81	5.16	0.04	0.01	9.52
TiO_2	-0.02	2.23	1.21	0.05	0.01	3.85	0.03	0.02	0.00	3.67	1.11	0.05
Cr_2O_3	-0.05	0.02	-0.03	0.03	0.00	0.06	0.00	0.00	0.00	0.02	0.02	0.00
Mno	-0.04	0.00	-0.04	1.10	0.00	0.02	0.90	0.87	0.00	0.13	0.00	1.66
FeO	0.02	19.60	1.10	34.71	0.05	15.98	32.56	30.95	0.06	20.49	1.90	28.45
Totale	100.08	94.35	94.90	100.70	99.79	95.33	100.44	100.31	99.71	94.99	95.17	100.55
Si	2.79	5.51	6.30	3.00	2.65	5.45	2.97	2.97	2.75	5.51	6.37	2.97
Ti	0.00	0.26	0.12	0.00	0.00	0.43	0.00	0.00	0.00	0.42	0.11	0.00
Al	1.21	3.25	5.30	1.98	1.34	3.23	2.01	2.02	1.24	3.18	5.08	2.01
Cr	0.00	0.00	0.00	0.00	0.00	0.01	0.00	0.00	0.00	0.00	0.00	0.00
Fe^{2+}	0.00	2.50	0.12	2.31	0.00	2.00	2.15	2.05	0.00	2.63	0.21	1.89
Mn	0.00	0.00	0.00	0.07	0.00	0.00	0.06	0.06	0.00	0.02	0.00	0.11
Mg	0.00	2.26	0.20	0.42	0.00	2.40	0.68	0.51	0.00	1.77	0.28	0.22
Ca	0.21	0.01	0.00	0.23	0.35	0.01	0.14	0.41	0.00	0.01	0.00	0.81
Na	0.80	0.04	0.13	0.00	0.64	0.04	0.01	0.01	0.25	0.03	0.08	0.01
K	0.00	1.60	1.63	0.00	0.01	1.87	0.00	0.00	0.73	1.81	1.75	0.00
Totale	5.01	15.43	13.81	8.01	5.00	15.44	8.02	8.02	4.98	15.38	13.89	8.03
Mg#		0.47	0.62	0.15		0.43	0.24	0.19		0.32	0.57	0.10
X_{Ab}	78.90				64.12				73.72			
X(Prp)				13.82			22.55	16.85				7.22
X(Alm)				76.26			70.83	67.73				62.36
X(Sps)				2.44			1.98	1.94				3.68
X(Grs)				7.48			4.64	13.48				26.74

Table 3.

Sample	372		367	
Amphibole	**Amp_2**		**Amp**	
	N=11	St Dev	N=28	St Dev
SiO_2	42.35	0.36	42.96	0.46
TiO_2	0.93	0.07	0.65	0.32
Al_2O_3	15.30	0.35	12.38	0.43
FeO*	13.07	0.38	16.77	0.26
MgO	10.41	0.31	9.98	0.24
MnO	0.05	0.01	0.31	0.02
CaO	12.07	0.08	11.12	0.21
Na_2O	1.37	0.05	1.97	0.16
K_2O	1.47	0.09	0.75	0.06
Sum	97.02	0.20	97.10	0.27
Plagioclase	**Pl_2**		**Pl**	
X_{Ab}	0.63	0.03	0.84	0.02
X_{An}	0.37	0.03	0.16	0.02
T(°C)	**670**	13	**644**	16
P(kbar)	**0.98**	0.03	**0.77**	0.04

Table 4.

	^{40}Ar	± 1σ	^{39}Ar	± 1σ	^{38}Ar	± 1σ	^{37}Ar	± 1σ	^{36}Ar	± 1σ	^{40}Ar*/^{39}Ar	± 1σ	Age	± 2σ	% error
Sample 240															
Biotite															
J values	**bk1a =**	**9.08530E-05**		**bk2a =**	**8.99830E-05**										
mcm115 bk1a	3231.53	176.89	128.21	5.97	2.35	0.98	19.90	17.98	-1.41	1.25	25.21	1.81	**372.00**	**24.22**	6.51
mcm115 bk1a	6361.78	130.14	230.52	6.53	3.16	0.67	9.05	9.24	-0.50	1.50	27.60	0.96	**403.63**	**12.76**	3.16
mcm115 bk1a	9278.25	313.63	334.80	8.65	3.73	0.83	19.15	6.00	-0.58	2.27	27.71	1.18	**405.14**	**15.54**	3.84
mcm115 bk2a	26670.60	604.51	947.70	13.79	11.76	1.79	171.60	12.64	5.35	3.19	28.14	0.76	**407.23**	**9.99**	2.45
mcm115 bk2a	77870.46	296.92	2757.76	41.13	33.35	1.58	32.96	17.00	7.92	1.68	28.24	0.43	**408.45**	**5.92**	1.45
mcm115 bk2a	63351.16	274.78	2234.32	38.21	29.67	1.33	71.48	17.02	6.01	1.42	28.35	0.50	**409.97**	**6.72**	1.64
mcm115 bk2a	17360.39	187.26	611.80	12.09	7.72	0.96	41.92	17.05	0.19	1.34	28.38	0.64	**410.25**	**8.46**	2.06
mcm115 bk2a	10035.02	190.36	352.96	9.09	5.44	1.02	53.12	17.05	0.86	1.42	28.43	0.91	**410.96**	**11.90**	2.90
mcm115 bk1a	1203.43	38.06	42.72	2.79	0.85	0.37	9.89	4.95	-1.58	1.02	28.17	2.05	**411.10**	**26.76**	6.51
mcm115 bk1a	2893.92	177.59	101.45	3.79	0.78	0.84	13.70	18.00	-0.74	1.33	28.53	2.05	**415.76**	**26.73**	6.43
mcm115 bk2a	32001.32	600.48	1106.36	14.76	16.94	1.91	419.26	12.63	4.62	3.19	28.92	0.67	**417.34**	**8.78**	2.10
mcm115 bk2a	94346.06	733.55	3254.13	28.38	45.26	2.22	66.60	12.62	7.14	3.29	28.99	0.34	**418.21**	**4.74**	1.13
mcm115 bk1a	14284.85	125.74	497.38	9.33	6.20	1.23	16.35	6.43	0.75	1.13	28.72	0.60	**418.28**	**7.96**	1.90
mcm115 bk1a	6455.00	130.39	224.15	6.99	3.96	0.67	23.89	9.23	1.01	1.61	28.80	1.07	**419.28**	**14.03**	3.35
mcm115 bk1a	14892.39	310.29	513.53	9.47	7.57	0.84	54.62	6.00	-0.65	2.30	29.00	0.81	**421.91**	**10.63**	2.52
mcm115 bk2a	100490.70	455.52	3400.04	30.42	42.40	1.76	34.22	17.00	5.22	1.77	29.56	0.30	**425.45**	**4.25**	1.00
mcm115 bk2a	61107.78	229.21	2020.24	21.69	27.05	1.58	102.64	17.02	2.39	1.51	30.25	0.34	**434.30**	**4.80**	1.10
mcm115 bk1a	19431.66	70.60	644.42	9.99	9.55	0.80	27.73	4.93	3.11	1.03	30.15	0.48	**436.82**	**6.47**	1.48
mcm115 bk1a	11768.46	122.38	382.13	9.14	5.38	1.22	25.46	6.42	1.94	1.18	30.80	0.80	**445.07**	**10.48**	2.35
mcm115 bk2a	18467.24	711.76	587.68	4.93	8.17	1.73	1.73	12.64	0.38	3.11	31.42	1.24	**449.24**	**15.81**	3.52
mcm115 bk1a	11671.73	123.08	371.39	8.10	6.36	1.27	20.90	6.42	1.92	1.27	31.43	0.76	**453.13**	**9.92**	2.19
mcm115 bk1a	17112.09	247.57	527.23	9.72	10.47	0.82	100.57	9.25	13.44	1.95	32.46	0.76	**466.20**	**9.85**	2.11
mcm115 bk1a	2443.29	165.62	74.79	2.80	0.50	0.29	-2.02	1.39	-3.15	0.69	32.67	2.53	**468.91**	**32.03**	6.83
mcm115 bk1a	13660.16	417.71	400.73	7.90	5.12	0.56	1.73	4.94	1.42	0.97	34.09	1.24	**486.73**	**15.67**	3.22
mcm115 bk1a	2263.26	117.10	65.68	3.04	1.09	1.15	-12.47	6.43	-0.31	1.09	34.46	2.39	**491.35**	**29.93**	6.09
mcm115 bk1a	3258.07	314.61	82.81	4.13	2.78	0.76	52.34	6.00	1.30	2.32	39.34	4.28	**551.34**	**51.69**	9.38
Sample 251															
White mica															
J values	**bk3b =**	**8.86780E-05**		**bk4b =**	**8.78080E-05**										
mcm115 bk3b	41056.91	937.25	1334.68	20.68	13.04	1.19	21.34	26.87	-13.97	3.82	30.76	0.85	**437.06**	**10.88**	2.49
mcm115 bk4b	66927.69	1044.87	2085.36	34.29	25.53	1.35	41.47	34.49	4.93	3.87	32.09	0.73	**449.87**	**9.25**	2.06
mcm115 bk4b	14665.49	813.71	438.79	9.17	6.39	1.00	53.83	34.55	-4.22	3.77	33.42	1.98	**466.28**	**24.45**	5.24
mcm115 bk4b	56278.05	824.24	1667.37	16.81	18.27	1.24	36.13	34.51	-0.54	3.91	33.75	0.60	**470.33**	**7.65**	1.63
mcm115 bk3b	159177.46	974.75	4701.88	32.35	49.54	2.27	32.29	26.80	5.48	4.53	33.85	0.31	**475.66**	**4.38**	0.92
mcm115 bk4b	29315.27	815.51	852.57	11.06	9.97	1.11	61.53	34.54	-3.84	3.77	34.38	1.06	**478.07**	**13.06**	2.73
mcm115 bk4b	74985.93	836.44	2159.38	32.34	27.37	1.60	45.39	34.45	3.66	3.91	34.73	0.65	**482.23**	**8.18**	1.70
mcm115 bk3a	305747.25	924.15	8778.45	74.31	95.19	2.19	30.19	23.28	1.37	2.89	34.83	0.31	**487.67**	**4.40**	0.90

mcm115 bk3a	264769.25	551.75	7540.60	35.32	82.89	1.99	47.96	23.29	1.75	2.09	35.11	0.18	**491.14**	**3.08**	0.63
mcm115 bk3a	281590.87	809.45	7963.65	45.08	85.05	2.17	17.41	12.39	0.17	2.01	35.36	0.22	**494.16**	**3.49**	0.71
mcm115 bk3a	191408.57	571.68	5412.50	37.30	60.21	2.08	127.54	12.39	6.80	2.01	35.36	0.27	**494.22**	**3.90**	0.79
mcm115 bk3a	271125.36	1034.19	7628.04	46.05	86.72	2.35	28.36	12.40	1.32	1.85	35.54	0.25	**496.40**	**3.78**	0.76
mcm115 bk4b	106629.52	831.94	2943.87	22.62	35.23	1.60	69.81	34.47	6.33	3.91	36.22	0.40	**500.36**	**5.26**	1.05

Biotite and biotite/white mica intergrowth

J values	**bk3a =**		**8.91130E-05**		**bk3b =**		**8.86780E-05**		**bk4a =**		**8.82430E-05**				
mcm115 bk3a	51851.66	286.76	1322.80	46.89	15.15	1.03	52.14	14.17	1.80	1.43	39.20	1.41	**540.49**	**16.92**	3.13
mcm115 bk4a	19698.77	99.21	451.65	9.80	4.91	0.62	-0.91	7.05	-0.35	1.27	43.61	0.97	**587.42**	**11.45**	1.95
mcm115 bk4a	13965.32	92.54	309.11	6.79	3.26	0.47	-0.35	7.04	1.85	1.12	45.18	1.04	**605.32**	**12.08**	2.00
mcm115 bk4a	18144.70	223.98	375.30	9.16	3.90	0.68	3.92	6.65	0.13	1.11	48.35	1.32	**641.02**	**15.00**	2.34
mcm115 bk4a	3029.93	88.03	61.61	1.94	0.65	0.42	2.31	7.06	-0.31	1.11	49.18	2.11	**650.24**	**23.58**	3.63
mcm115 bk3a	4476.46	413.58	91.92	4.52	3.41	1.05	290.23	12.42	2.77	1.78	48.70	5.10	**650.28**	**57.22**	8.80
mcm115 bk4a	16214.71	95.00	329.28	7.47	3.65	0.52	9.09	7.06	-1.11	1.25	49.24	1.15	**650.98**	**13.09**	2.01
mcm115 bk3a	9148.36	251.46	185.01	6.75	2.17	0.57	44.87	23.35	-1.26	1.83	49.45	2.26	**658.65**	**25.35**	3.85
mcm115 bk4a	33380.67	236.05	660.61	10.81	7.07	0.82	-0.53	6.63	0.04	1.19	50.53	0.90	**665.21**	**10.30**	1.55
mcm115 bk3a	108384.42	359.08	1990.27	18.86	23.17	1.32	240.01	23.32	2.70	1.95	54.46	0.55	**713.70**	**6.61**	0.93
mcm115 bk3b	82468.81	962.76	1508.97	32.35	14.87	1.15	50.15	26.86	-9.23	3.94	54.65	1.33	**715.82**	**14.72**	2.06
mcm115 bk4a	7203.05	89.74	130.12	4.95	1.38	0.47	2.09	7.06	0.70	1.13	55.35	2.22	**717.57**	**23.90**	3.33
mcm115 bk3a	68926.96	210.81	1240.31	14.99	15.76	0.96	100.81	21.16	2.04	1.83	55.57	0.69	**725.74**	**8.02**	1.11
mcm115 bk3a	70480.76	229.34	1250.89	14.03	25.97	1.20	30.75	21.16	0.92	1.83	56.34	0.66	**734.02**	**7.66**	1.04
mcm115 bk3a	97414.54	271.97	1728.87	16.90	20.97	1.11	31.41	21.18	1.77	1.76	56.35	0.57	**734.03**	**6.83**	0.93
mcm115 bk3a	107507.70	295.27	1902.78	42.12	23.75	1.11	50.57	21.19	-0.81	2.73	56.50	1.26	**735.69**	**13.81**	1.88
mcm115 bk4a	42187.30	186.98	714.28	10.96	7.08	0.65	9.86	5.27	0.57	1.07	59.06	0.94	**756.79**	**10.35**	1.37
mcm115 bk4a	32621.54	235.31	551.43	9.16	6.44	0.74	16.15	6.65	0.16	1.17	59.16	1.07	**757.79**	**11.62**	1.53
mcm115 bk3b	80366.68	519.26	1354.74	52.79	14.92	1.02	44.84	31.61	0.44	2.51	59.32	2.34	**765.62**	**24.84**	3.24
mcm115 bk3a	94735.65	301.62	1591.60	15.03	27.40	1.32	71.33	23.33	2.90	1.95	59.52	0.59	**767.71**	**6.97**	0.91
mcm115 bk3b	28864.94	429.58	480.34	8.89	5.50	0.81	32.38	31.71	-2.93	2.31	60.09	1.43	**773.70**	**15.27**	1.97
mcm115 bk3a	331574.29	794.32	5493.61	29.49	74.34	2.19	118.56	23.31	5.19	2.09	60.36	0.35	**776.45**	**4.87**	0.63
mcm115 bk4a	19960.87	116.91	324.90	7.18	3.67	0.51	8.76	7.03	2.51	1.13	61.44	1.40	**781.48**	**14.84**	1.90
mcm115 bk4a	28659.64	232.49	466.25	8.58	5.66	0.76	29.42	6.64	-0.15	1.13	61.47	1.24	**781.79**	**13.14**	1.68
mcm115 bk3b	46774.61	444.88	756.82	22.55	6.48	0.74	5.07	31.70	-1.52	2.29	61.80	1.93	**791.52**	**20.29**	2.56
mcm115 bk4a	26554.57	107.44	423.03	8.64	5.47	0.64	2.27	7.04	2.42	1.17	62.77	1.31	**795.21**	**13.77**	1.73
mcm115 bk4a	3768.84	219.48	59.07	2.11	0.71	0.54	14.36	6.65	1.14	0.96	63.80	4.36	**805.73**	**44.51**	5.52
mcm115 bk3a	4285.40	413.11	67.61	4.16	1.04	1.06	85.89	12.44	-1.91	1.57	63.39	7.25	**807.87**	**74.55**	9.23
mcm115 bk3b	170066.90	991.68	2664.04	20.68	29.56	1.53	70.61	26.85	-3.15	4.03	63.84	0.62	**812.49**	**7.14**	0.88
mcm115 bk4a	26073.32	242.44	400.92	3.70	4.09	0.68	-2.54	6.63	-0.58	1.15	65.03	0.85	**818.23**	**9.23**	1.13
mcm115 bk3a	593071.79	1790.69	9044.95	44.11	102.68	2.62	107.68	12.40	6.50	2.25	65.57	0.38	**830.14**	**5.06**	0.61
mcm115 bk4a	28845.26	227.53	431.37	8.77	4.23	0.67	11.17	6.64	-0.03	1.13	66.87	1.46	**836.70**	**14.98**	1.79
mcm115 bk3b	273335.66	1073.61	4073.29	28.45	46.13	1.90	198.87	26.83	7.24	4.18	67.10	0.54	**845.65**	**6.38**	0.75
mcm115 bk3b	79109.49	458.16	1178.88	14.77	13.24	0.98	55.41	31.68	1.16	2.40	67.11	0.93	**845.67**	**9.91**	1.17
mcm115 bk3a	6669.88	172.28	98.73	3.99	2.39	0.73	323.91	21.20	1.22	1.76	67.56	3.24	**850.21**	**32.70**	3.85
mcm115 bk3a	2432.02	171.58	35.31	3.61	-2.26	0.97	17.14	21.23	-0.63	1.70	68.88	8.56	**863.43**	**85.37**	9.89
mcm115 bk4a	68908.12	234.43	947.76	19.66	11.04	0.74	15.42	5.26	0.38	1.13	72.71	1.53	**894.21**	**15.23**	1.70
mcm115 bk4a	3928.96	167.41	54.00	3.89	0.22	0.30	3.50	5.27	-1.52	0.91	72.76	6.08	**894.68**	**59.10**	6.61
mcm115 bk3b	412982.38	1322.26	5699.37	32.35	68.50	1.80	59.45	26.76	11.52	4.13	72.46	0.47	**898.76**	**5.81**	0.65
mcm115 bk3b	339370.09	1184.85	4636.05	30.40	52.54	1.80	63.59	26.78	8.14	4.24	73.20	0.54	**905.98**	**6.38**	0.70

mcm115 bk4a	17211.40	174.64	230.72	6.43	3.15	0.47	17.83	5.27	-0.72	0.93	74.60	2.21	**912.46**	**21.55**	2.36
mcm115 bk3b	3801.43	428.09	51.24	2.43	1.72	0.70	521.46	31.64	3.91	2.46	74.18	9.07	**915.51**	**87.82**	9.59

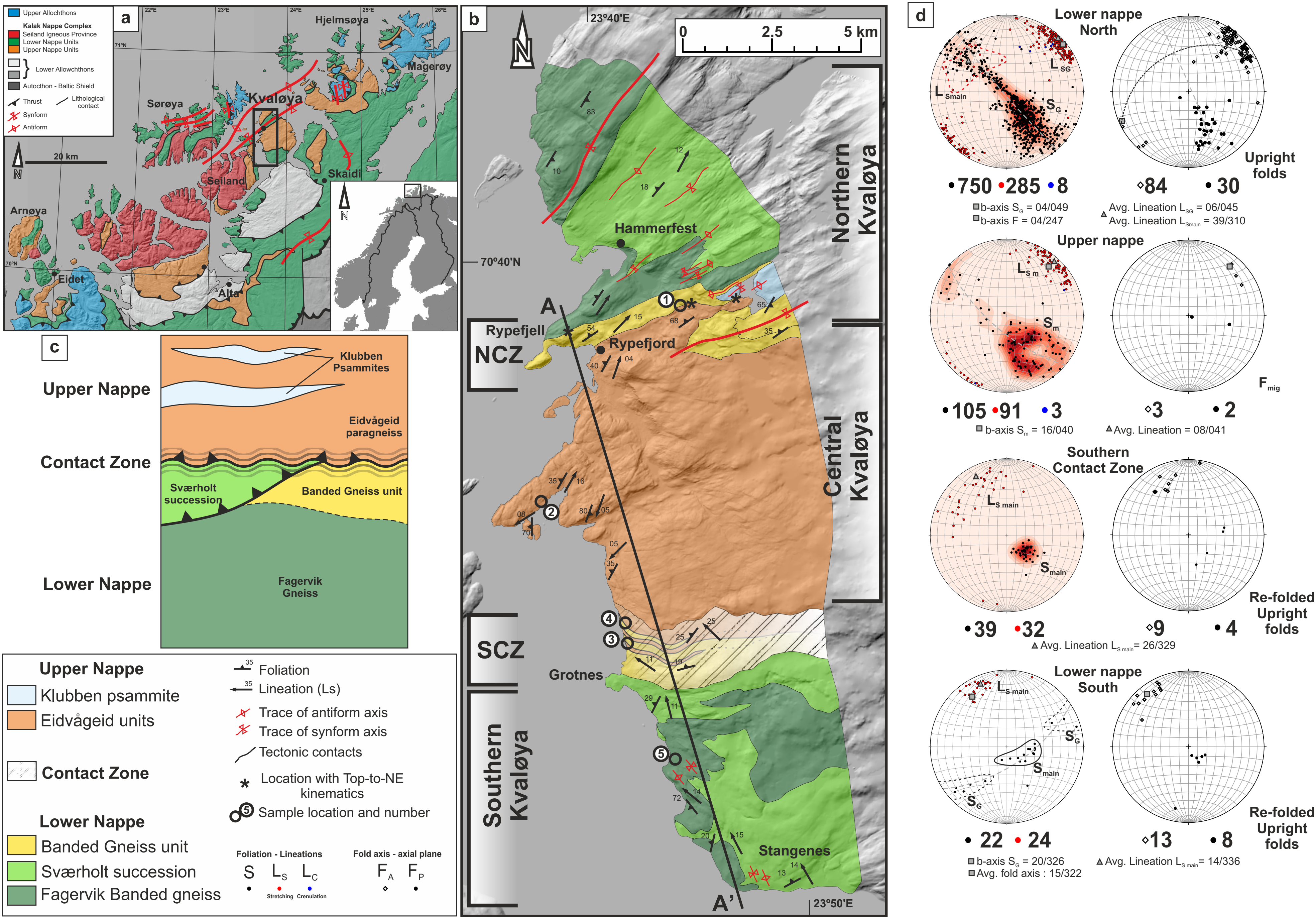

a
Upper Allochthons
Kalak Nappe Complex
Seiland Igneous Province
Lower Nappe Units
Upper Nappe Units
Lower Allowchthons
Autochton - Baltic Shield
Thrust
Lithological contact
Synform
Antiform
Hjelmsøya
Magerøy
Sørøya
Kvaløya
Skaidi
Seiland
Arnøya
Eidet
Alta
20 km
b
23°40'E
0 2.5 5 km
Hammerfest
70°40'N
Rypefjell
Rypefjord
NCZ
SCZ
Grotnes
Stangenes
Northern Kvaløya
Central Kvaløya
Southern Kvaløya
A
A'
23°50'E
c
Upper Nappe
Klubben Psammites
Eidvågeid paragneiss
Contact Zone
Sværholt succession
Banded Gneiss unit
Lower Nappe
Fagervik Gneiss
Upper Nappe
Klubben psammite
Eidvågeid units
Contact Zone
Lower Nappe
Banded Gneiss unit
Sværholt succession
Fagervik Banded gneiss
Foliation
Lineation (Ls)
Trace of antiform axis
Trace of synform axis
Tectonic contacts
Location with Top-to-NE kinematics
Sample location and number
Foliation - Lineations
Fold axis - axial plane
S
L_S
L_C
Stretching
Crenulation
F_A
F_P
d
Lower nappe North
L_{SG}
L_{Smain}
S_G
Upright folds
750 285 8
84 30
b-axis S_G = 04/049
b-axis F = 04/247
Avg. Lineation L_{SG} = 06/045
Avg. Lineation L_{Smain} = 39/310
Upper nappe
$L_{S m}$
S_m
F_{mig}
105 91 3
3 2
b-axis S_m = 16/040
Avg. Lineation = 08/041
Southern Contact Zone
$L_{S main}$
S_{main}
Re-folded Upright folds
39 32
9 4
Avg. Lineation $L_{S main}$ = 26/329
Lower nappe South
$L_{S main}$
S_G
S_{main}
Re-folded Upright folds
22 24
13 8
b-axis S_G = 20/326
Avg. fold axis : 15/322
Avg. Lineation $L_{S main}$ = 14/336

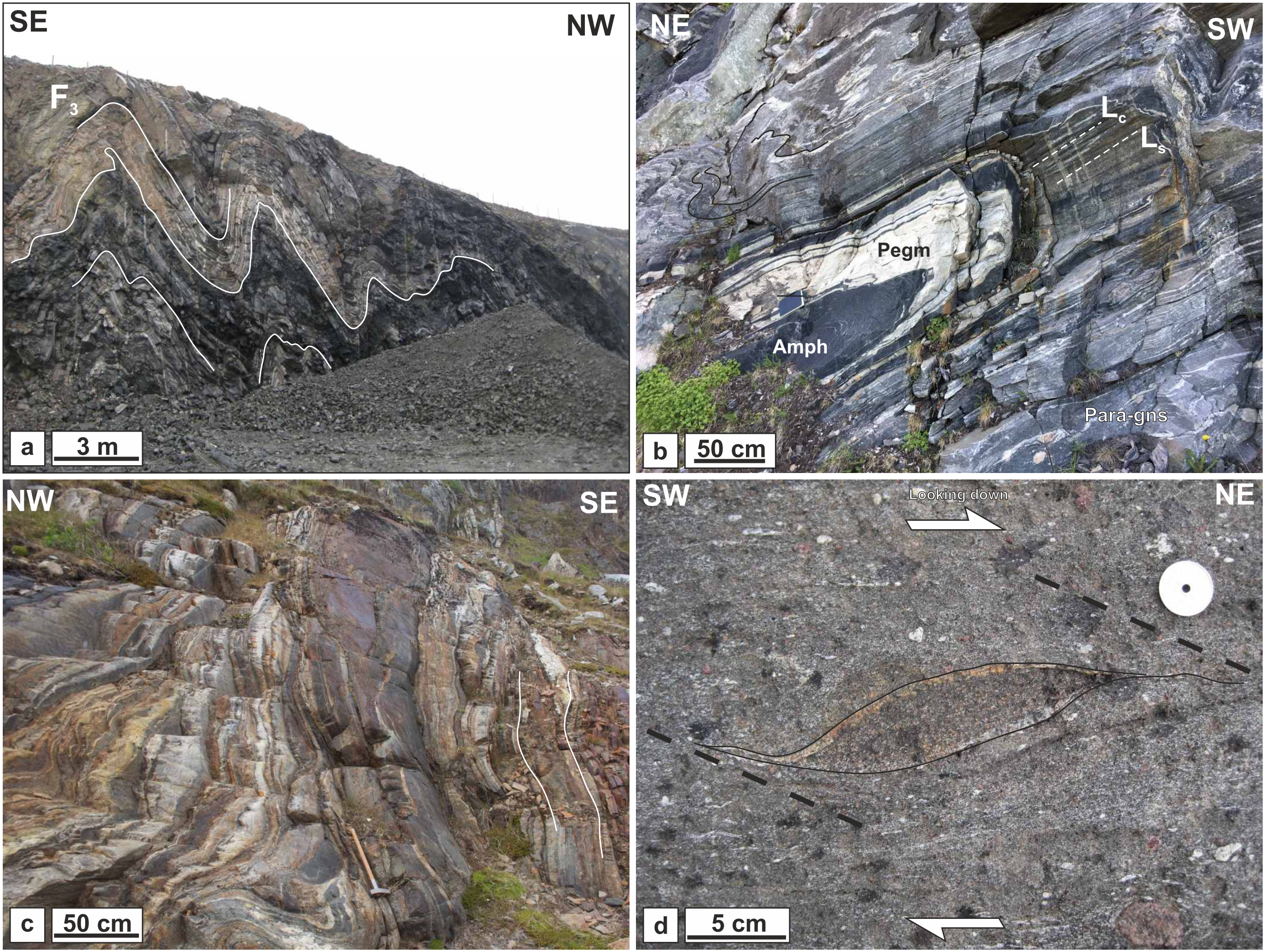
SE
NW
F3
a
3 m
NE
SW
Lc
Ls
Pegm
Amph
Para-gns
b
50 cm
NW
SE
c
50 cm
SW
NE
Looking down
d
5 cm

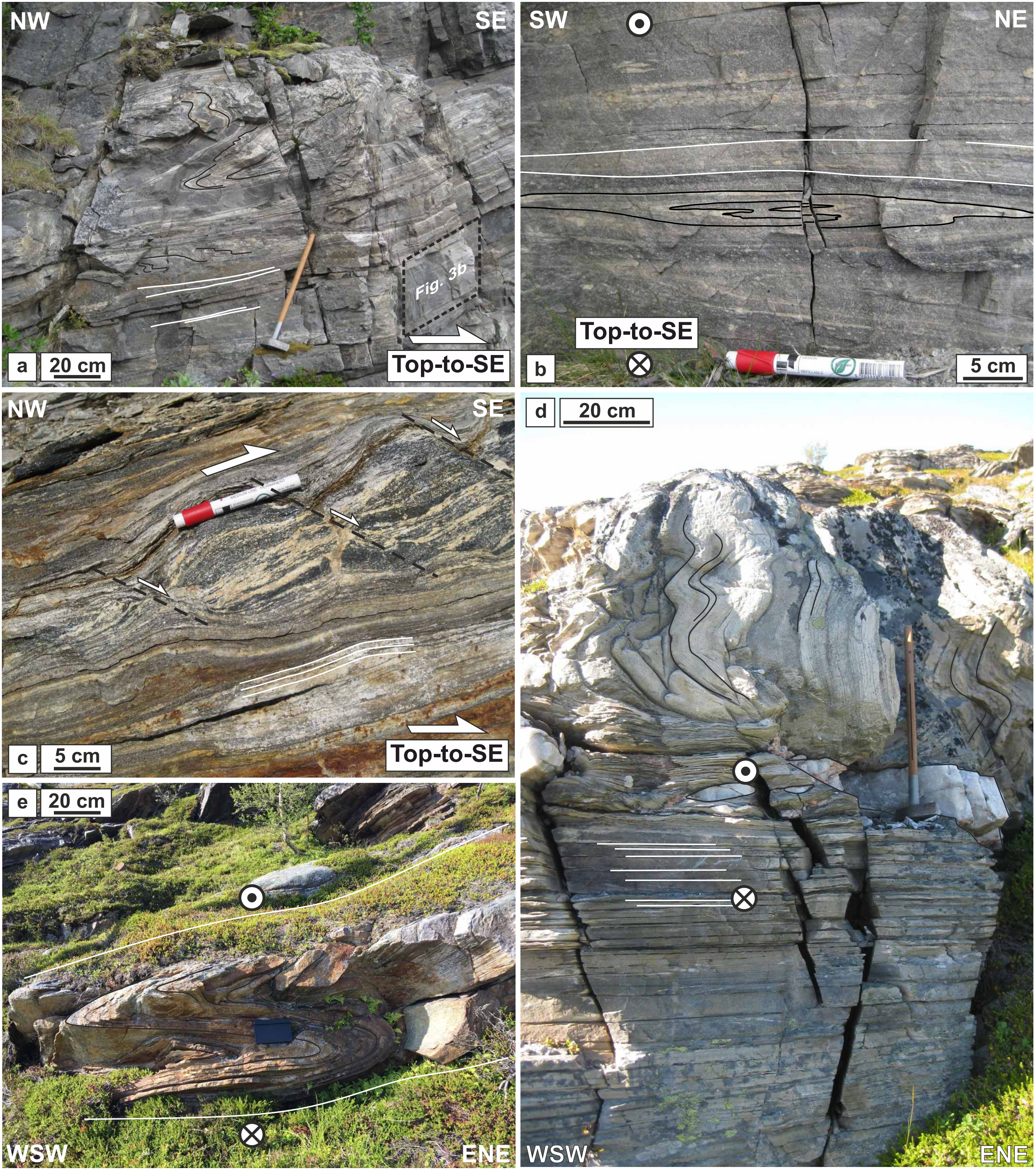

NW
SE
Fig. 3b
a
20 cm
Top-to-SE
SW
NE
b
Top-to-SE
5 cm
NW
SE
c
5 cm
Top-to-SE
d
20 cm
WSW
ENE
e
20 cm
WSW
ENE

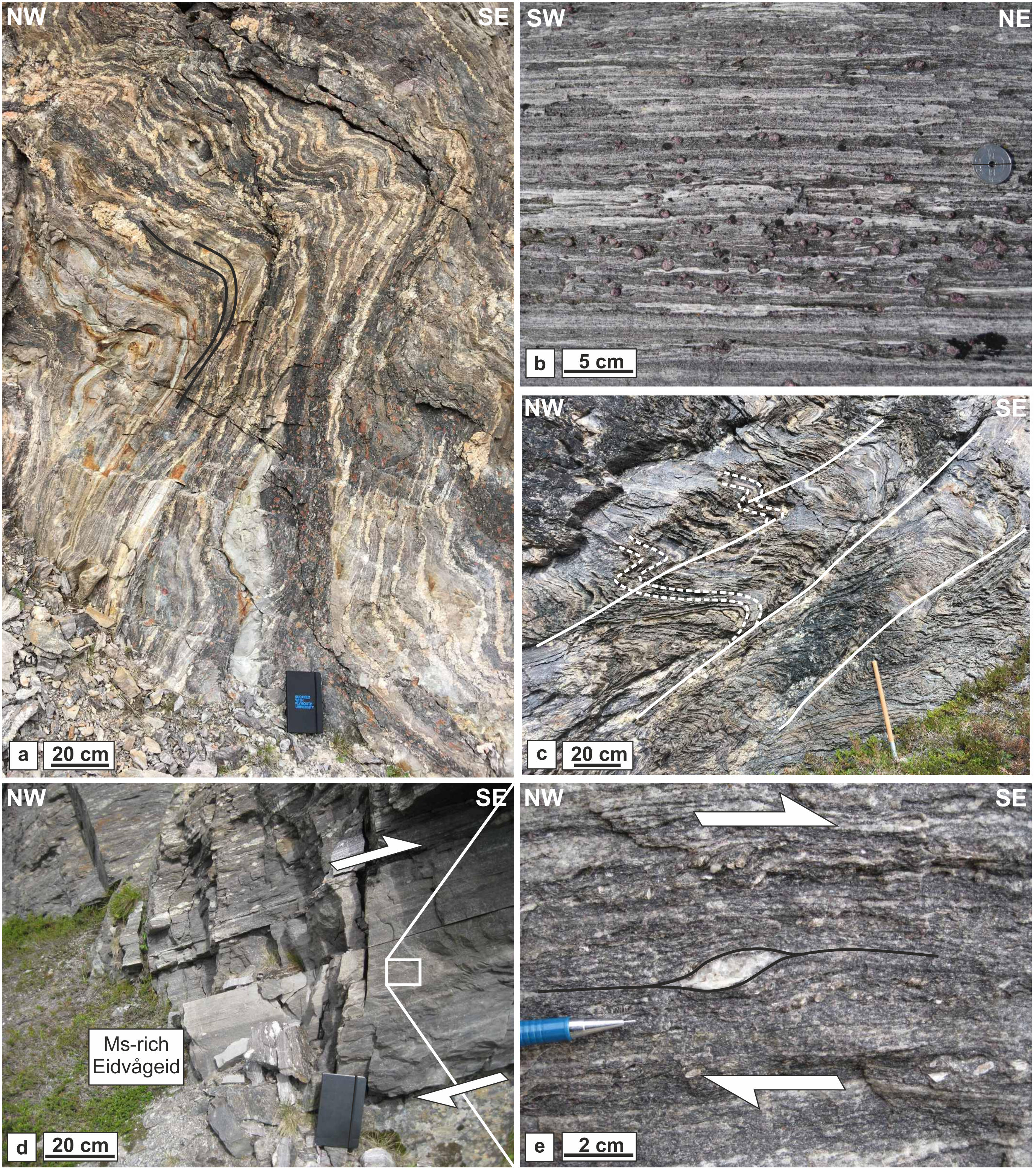
NW
SE
a
20 cm
SW
NE
b
5 cm
NW
SE
c
20 cm
NW
SE
Ms-rich
Eidvågeid
d
20 cm
NW
SE
e
2 cm

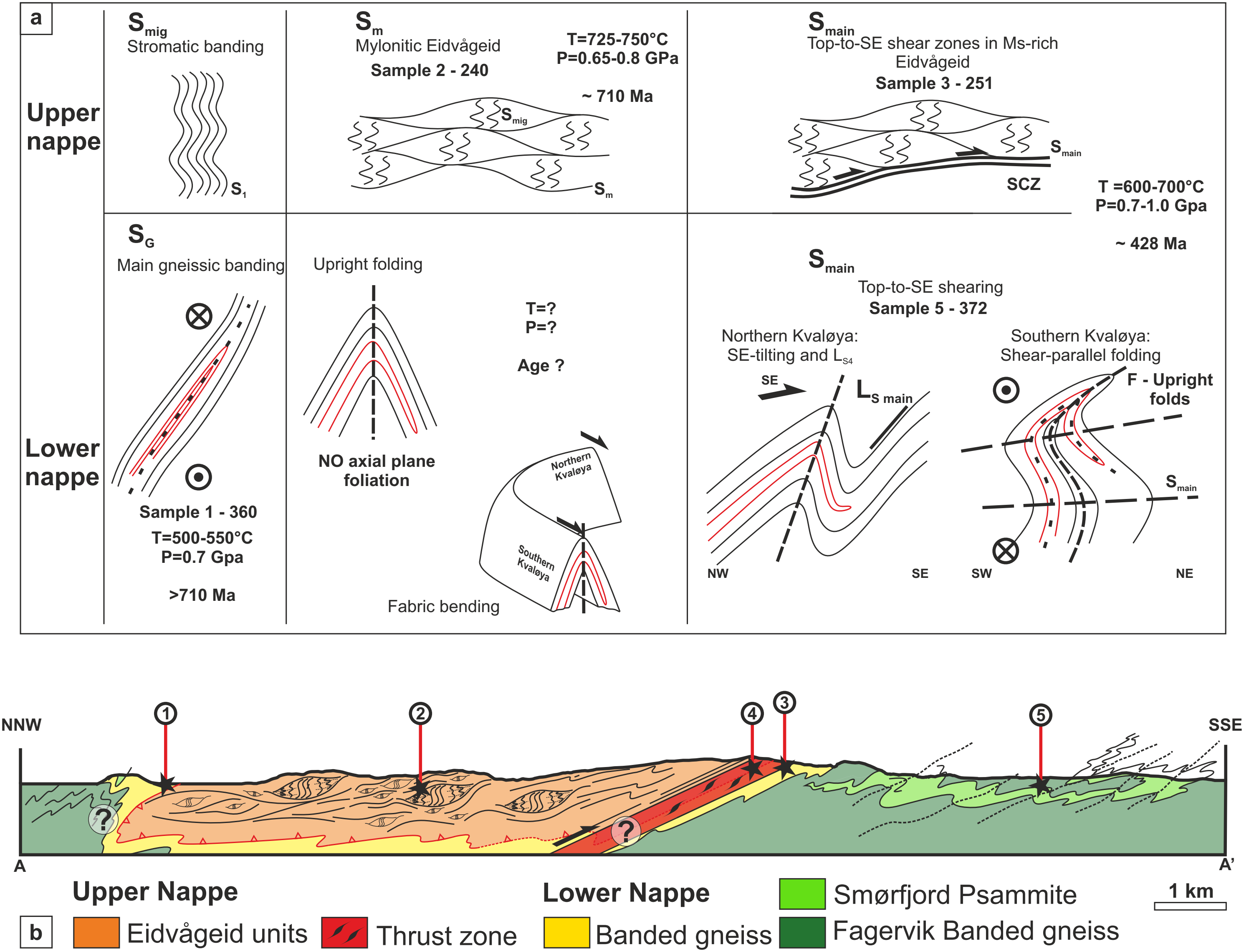

a
Upper nappe
Lower nappe
S mig
Stromatic banding
S1
S m
Mylonitic Eidvågeid
Sample 2 - 240
T=725-750°C
P=0.65-0.8 GPa
~ 710 Ma
S mig
S m
S main
Top-to-SE shear zones in Ms-rich Eidvågeid
Sample 3 - 251
S main
SCZ
T =600-700°C
P=0.7-1.0 Gpa
~ 428 Ma
S G
Main gneissic banding
Sample 1 - 360
T=500-550°C
P=0.7 Gpa
>710 Ma
Upright folding
NO axial plane foliation
T=?
P=?
Age ?
Northern Kvaløya
Southern Kvaløya
Fabric bending
S main
Top-to-SE shearing
Sample 5 - 372
Northern Kvaløya:
SE-tilting and L S4
SE
L S main
NW
SE
Southern Kvaløya:
Shear-parallel folding
F - Upright folds
S main
SW
NE
b
NNW
SSE
1
2
3
4
5
A
A'
Upper Nappe
Eidvågeid units
Thrust zone
Lower Nappe
Banded gneiss
Smørfjord Psammite
Fagervik Banded gneiss
1 km

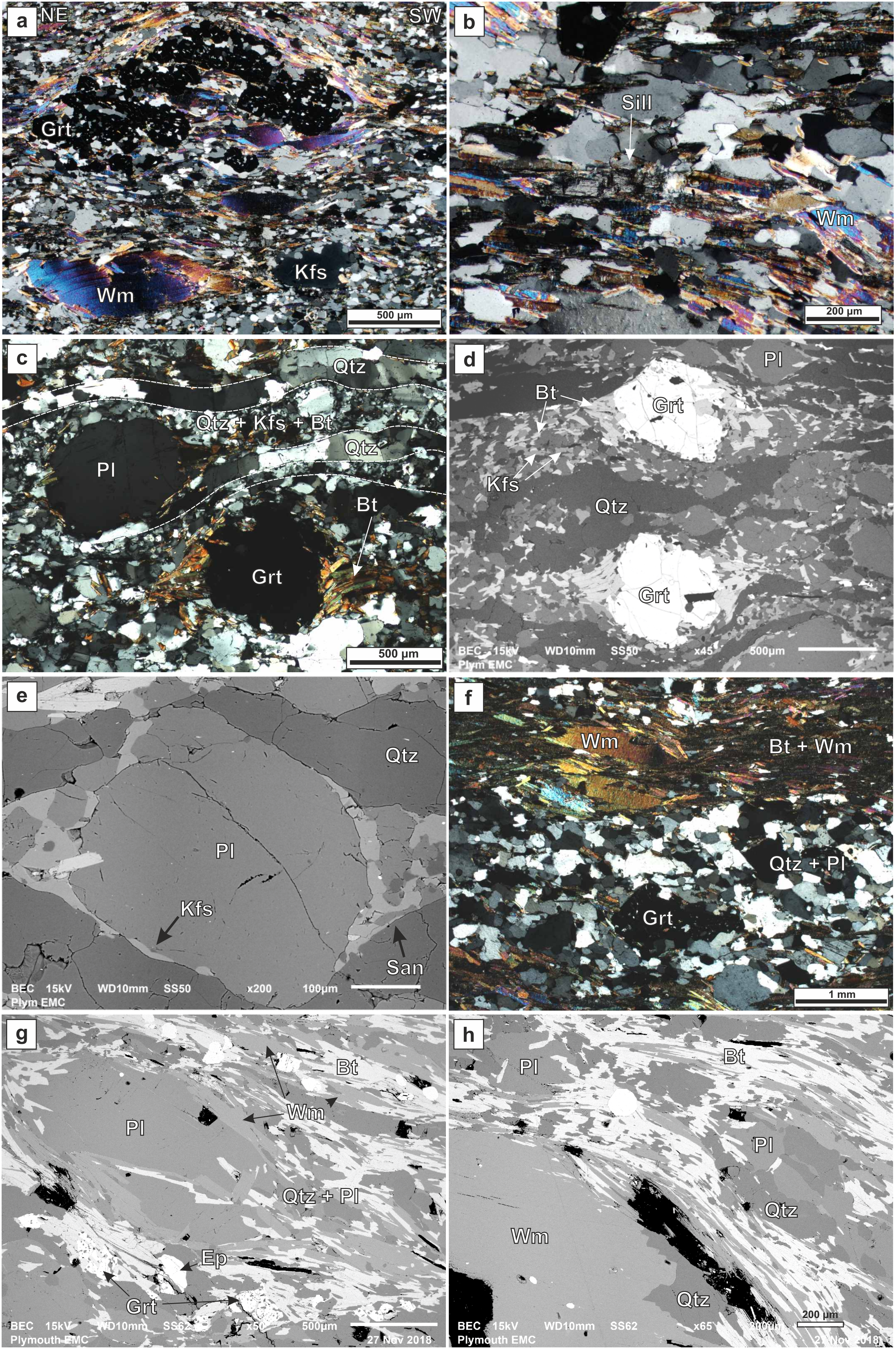
a
NE
SW
Grt
Kfs
Wm
500 µm
b
Sill
Wm
200 µm
c
Qtz
Qtz + Kfs + Bt
Qtz
Pl
Bt
Grt
500 µm
d
Pl
Bt
Grt
Kfs
Qtz
Grt
BEC 15kV WD10mm SS50 x45 500µm
Plym EMC
e
Qtz
Pl
Kfs
San
BEC 15kV WD10mm SS50 x200 100µm
Plym EMC
f
Wm
Bt + Wm
Qtz + Pl
Grt
1 mm
g
Bt
Wm
Pl
Qtz + Pl
Ep
Grt
BEC 15kV WD10mm SS62 x50 500µm 27 Nov 2018
Plymouth EMC
h
Bt
Pl
Pl
Qtz
Wm
Qtz
200 µm
BEC 15kV WD10mm SS62 x65
Plymouth EMC

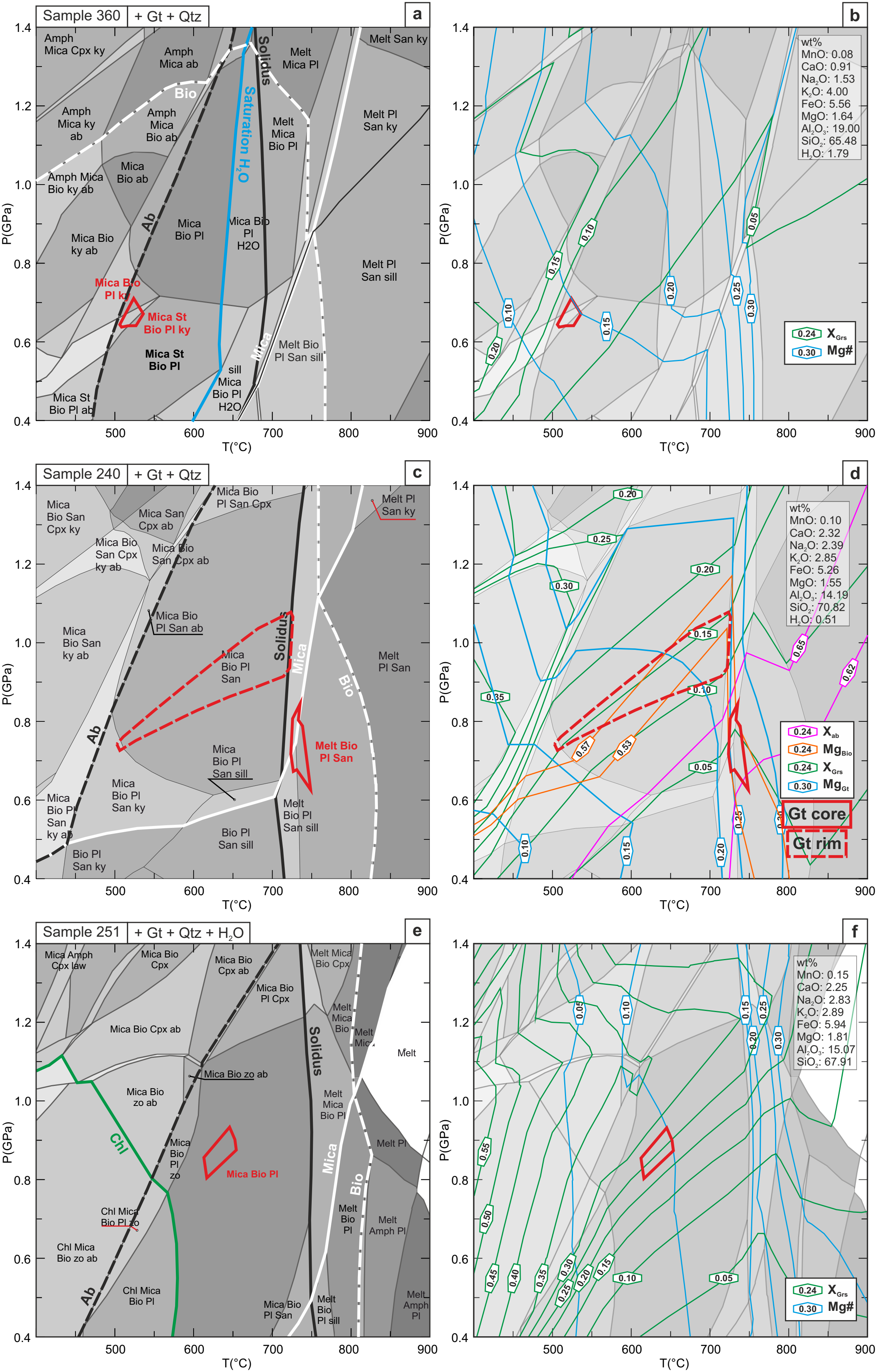

Sample 360
+ Gt + Qtz
a
b
Solidus
Saturation H_2O
Bio
Ab
Mica
Mica Bio Pl ky
Mica St Bio Pl ky
Mica St Bio Pl
wt%
MnO: 0.08
CaO: 0.91
Na_2O: 1.53
K_2O: 4.00
FeO: 5.56
MgO: 1.64
Al_2O_3: 19.00
SiO_2: 65.48
H_2O: 1.79
X_{Grs}
Mg#
Sample 240
+ Gt + Qtz
c
d
Melt Bio Pl San
wt%
MnO: 0.10
CaO: 2.32
Na_2O: 2.39
K_2O: 2.85
FeO: 5.26
MgO: 1.55
Al_2O_3: 14.19
SiO_2: 70.82
H_2O: 0.51
X_{ab}
Mg_{Bio}
X_{Grs}
Mg_{Gt}
Gt core
Gt rim
Sample 251
+ Gt + Qtz + H_2O
e
f
Chl
Mica Bio Pl
wt%
MnO: 0.15
CaO: 2.25
Na_2O: 2.83
K_2O: 2.89
FeO: 5.94
MgO: 1.81
Al_2O_3: 15.07
SiO_2: 67.91
P(GPa)
T(°C)

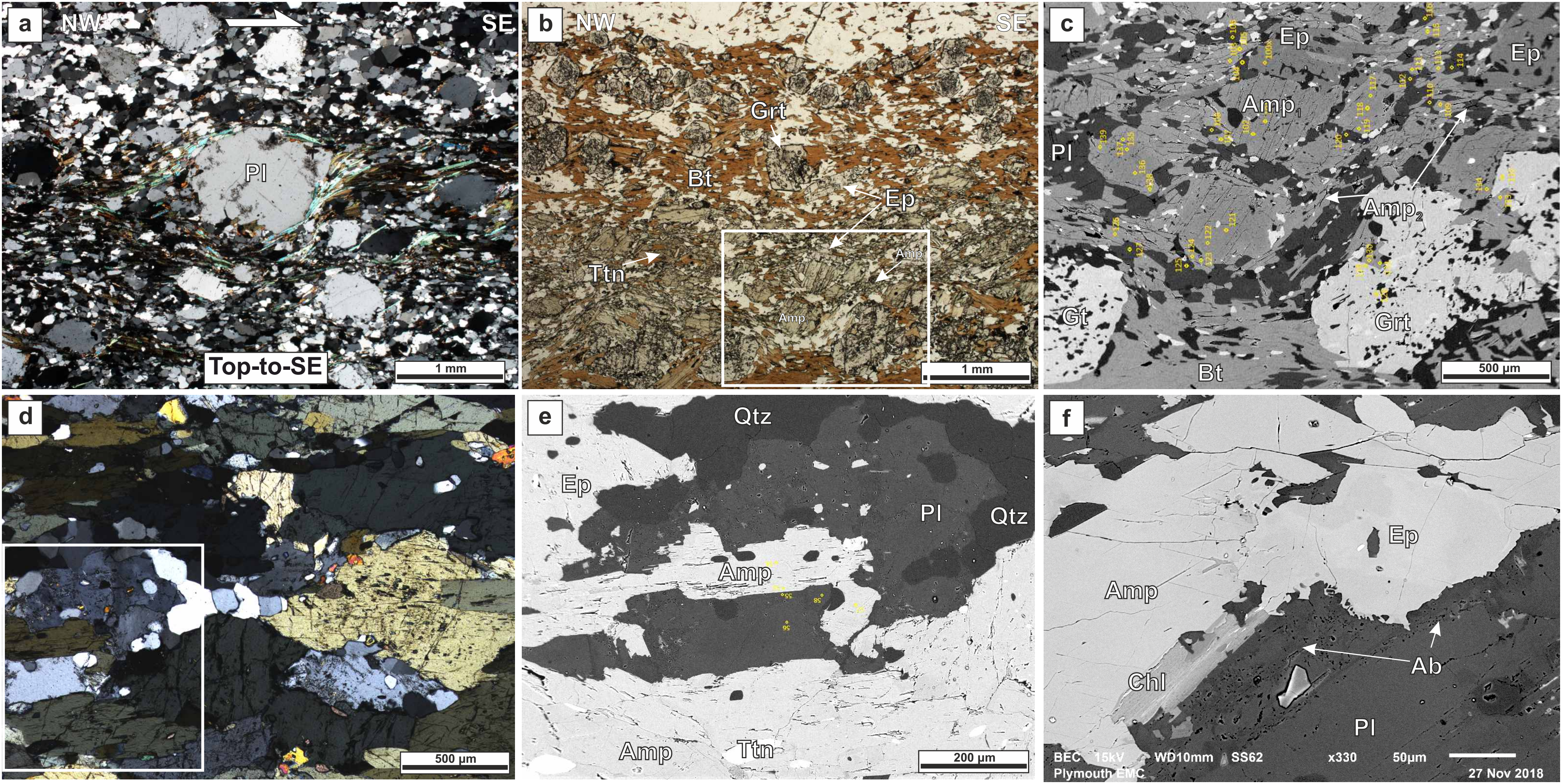

a
NW
SE
Pl
Top-to-SE
1 mm
b
NW
SE
Grt
Bt
Ep
Ttn
Amp
Amp
1 mm
c
Ep
Ep
Amp1
Pl
Amp2
Gt
Grt
Bt
500 µm
d
500 µm
e
Qtz
Ep
Pl
Qtz
Amp
Amp
Ttn
200 µm
f
Ep
Amp
Ab
Chl
Pl
BEC 15kV WD10mm SS62 x330 50µm
Plymouth EMC
27 Nov 2018

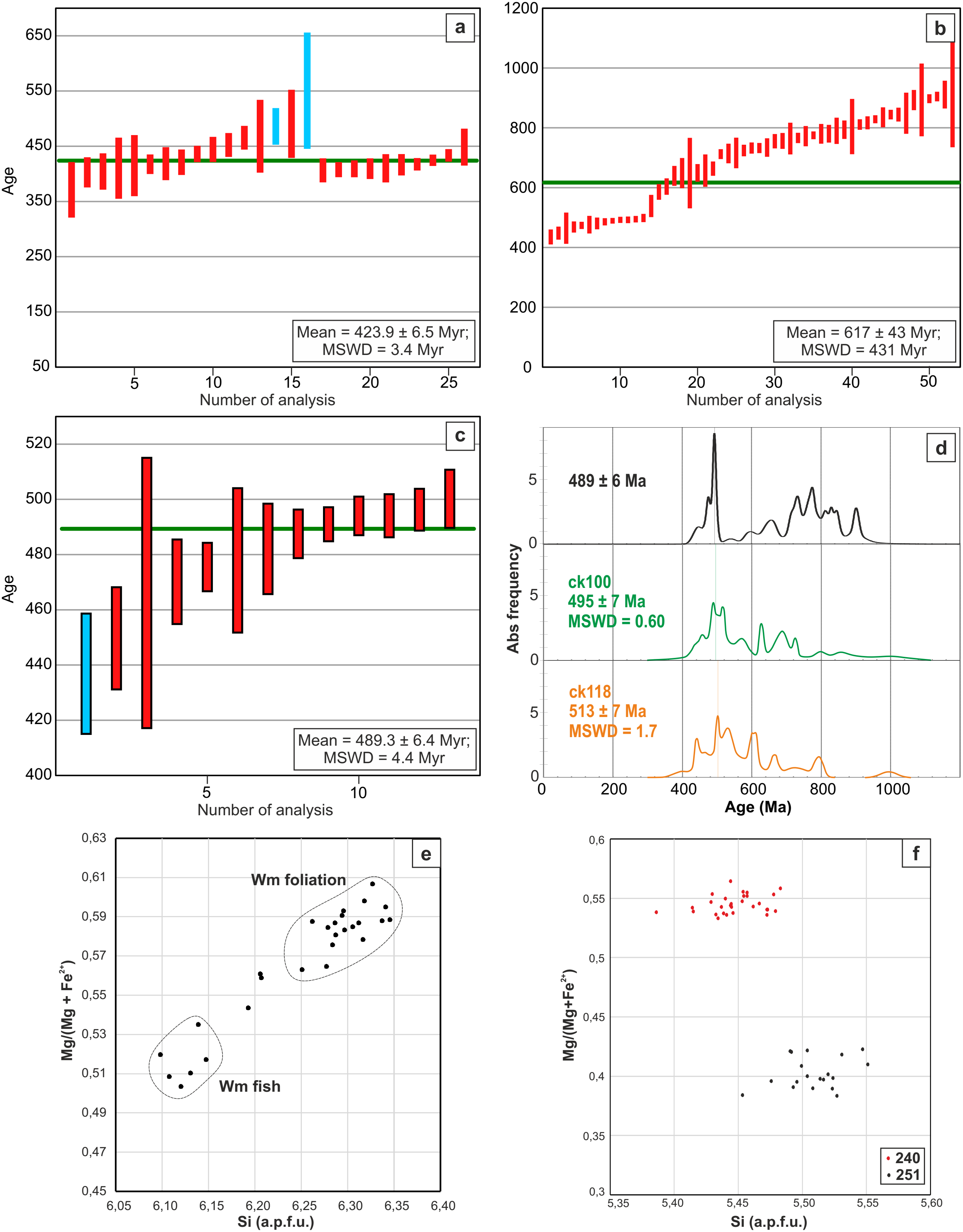
a
Mean = 423.9 ± 6.5 Myr;
MSWD = 3.4 Myr
Age
Number of analysis
b
Mean = 617 ± 43 Myr;
MSWD = 431 Myr
Number of analysis
c
Mean = 489.3 ± 6.4 Myr;
MSWD = 4.4 Myr
Age
Number of analysis
d
489 ± 6 Ma
ck100
495 ± 7 Ma
MSWD = 0.60
ck118
513 ± 7 Ma
MSWD = 1.7
Abs frequency
Age (Ma)
e
Wm foliation
Wm fish
Mg/(Mg + Fe2+)
Si (a.p.f.u.)
f
240
251
Mg/(Mg+Fe2+)
Si (a.p.f.u.)

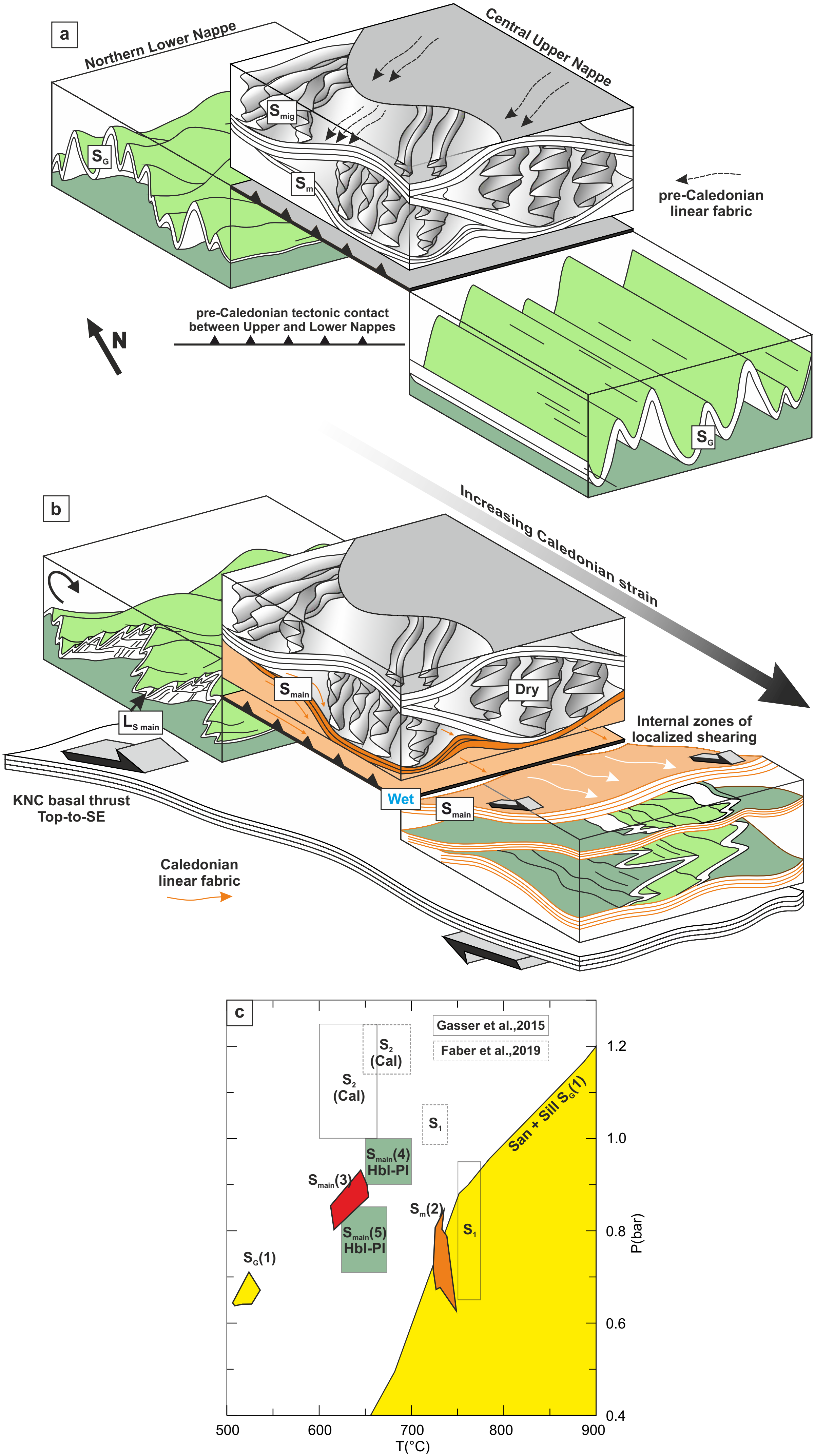

a
Northern Lower Nappe
Central Upper Nappe
S_{mig}
S_G
S_m
pre-Caledonian linear fabric
pre-Caledonian tectonic contact between Upper and Lower Nappes
N
S_G
b
Increasing Caledonian strain
S_{main}
Dry
Internal zones of localized shearing
$L_{S\ main}$
KNC basal thrust Top-to-SE
Wet
S_{main}
Caledonian linear fabric
c
Gasser et al.,2015
Faber et al.,2019
S_2 (Cal)
S_2 (Cal)
S_1
S_{main}(4) Hbl-Pl
S_{main}(3)
S_m(2)
S_1
S_{main}(5) Hbl-Pl
S_G(1)
San + Sill S_G(1)
1.2
1.0
0.8
0.6
0.4
P(bar)
500
600
700
800
900
T(°C)

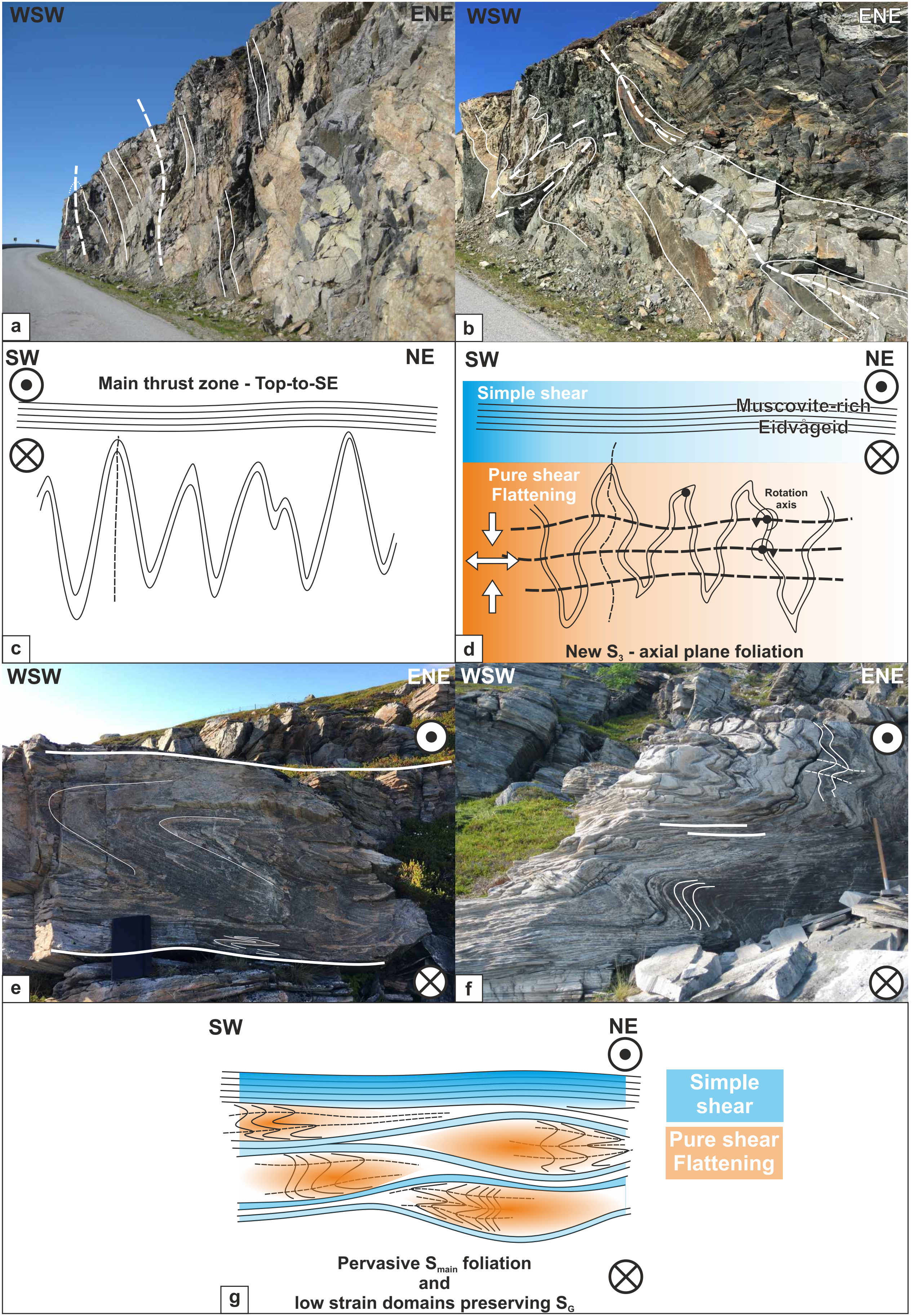
WSW
ENE
a
WSW
ENE
b
SW
NE
Main thrust zone - Top-to-SE
c
SW
NE
Simple shear
Muscovite-rich
Eidvågeid
Pure shear
Flattening
Rotation axis
New S_3 - axial plane foliation
d
WSW
ENE
e
WSW
ENE
f
SW
NE
Simple shear
Pure shear
Flattening
Pervasive S_{main} foliation
and
low strain domains preserving S_G
g

Author Statement

Alberto Ceccato: conceptualization, investigation, formal analysis, data curation, visualization, writing – original draft, review & editing; Luca Menegon: conceptualization, investigation, resources, project administration, funding acquisition, writing – original draft, review & editing; Clare J. Warren: investigation, resources, formal analysis, validation, data curation, writing – review & editing; Alison M. Halton: investigation, resources, formal analysis, validation, data curation.

Supplementary Material.

Methods: Analytical details.

Thin sections were carbon coated before SEM analysis. The working conditions for both SEM and EMPA (Open University) analysis were 20 keV accelerating voltage and 20 nA beam current; 2 µm spot size. The working conditions during EMPA analysis at the Department of Lithospheric Research of the University of Vienna (Austria) were 15 keV accelerating voltage and 20-25 nA beam current. Garnet and feldspar analysis were performed with a focused beam with 1 µm spot size. White mica and biotite were analysed with a defocussed beam with 5 and 3 µm spot size, respectively.

In the pseudosection calculations, the amount of aqueous fluid was taken from loss on ignition and considered as a pure phase. Selected end-members have been systematically excluded from calculation: margarite (ma) for Mica(W); microcline (mic) for San; andradite for Gt(WPH).

In-situ UV Laser $^{40}Ar/^{39}Ar$ geochronology. Samples were irradiated at the McMaster University Reactor (Canada) for 300 MWH along with standard GA1550 (99.738 +/- 0.104 Ma Renne et al 2011). The standard run was GA1550 (age 99.738+/- 0.104Ma (Renne et al 2011)), and the error on the calculated J values was 1% - this error on the J value is propagated into the calculated ages. Day to day machine stability is monitored via the background measurements rather than standards for Ar measurement (again average of the background measurements subtracted from the data and error based on standard deviation of these measurements propagated in the age error calculations). The gas clean-up and inlet was fully automated, with measurement of ^{40}Ar, ^{39}Ar, ^{38}Ar, ^{37}Ar, and ^{36}Ar, each for ten scans, and the final measurements were extrapolations back to the inlet time. Data were processed using inhouse software to correct for mass spectrometer discrimination (using a $^{40}Ar/^{36}Ar$ discrimination of 305.2), decay of ^{39}Ar since irradiation, and neutron-induced interference reactions (^{40}Ar from potassium $(^{40}Ar/^{39}Ar)_K = 0.0085 \pm 0.0000425$). Blank measurements made between every 1-2 analysis were subtracted from the measurement data. ^{36}Ar contents were at background level so correction for atmospheric argon was not made to the data. Ages were calculated using the decay constants of Renne et al., 2011 and J values used listed in Table 4. All ages are reported at the 2σ level and include a 0.5% error on the J value.

Figures Supplementary Material.

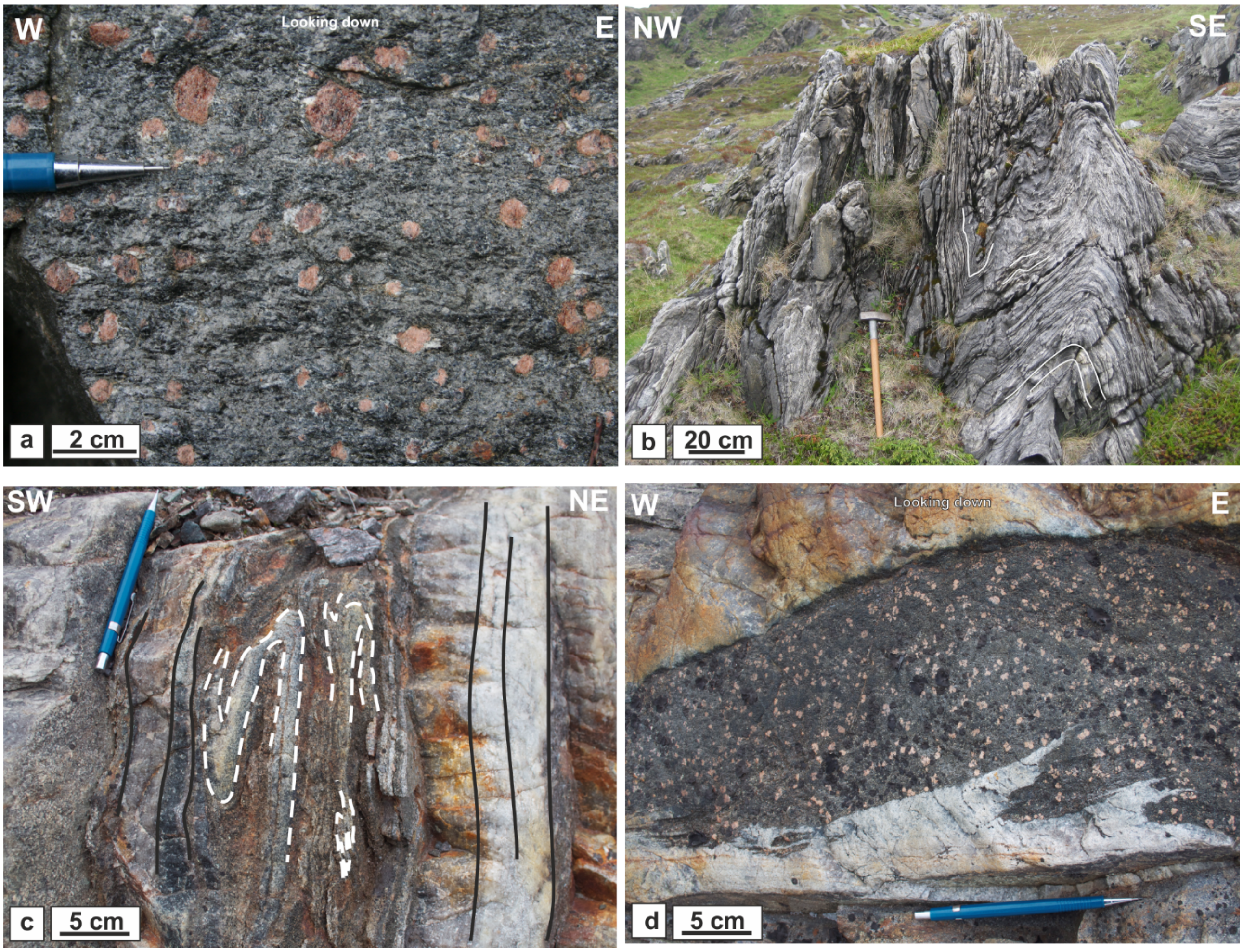

Figure SM1. (a) Detail of Gt-bearing amphibolite in the Fagervik gneiss complex. Grt are usually surrounded by quartzo-feldspatic haloes and strain shadows. (b) Upright folds re-folding the main fabric (white solid lines) in the Sværholt Psammite on the southwestern shore of Rypefjell. (c) Detail of isoclinal, rootless folds (dashed white lines) embedded in the gneissic fabric of the banded gneiss unit (black lines). (d) Detail of Grt-amphibolite

layers in the banded gneiss unit.

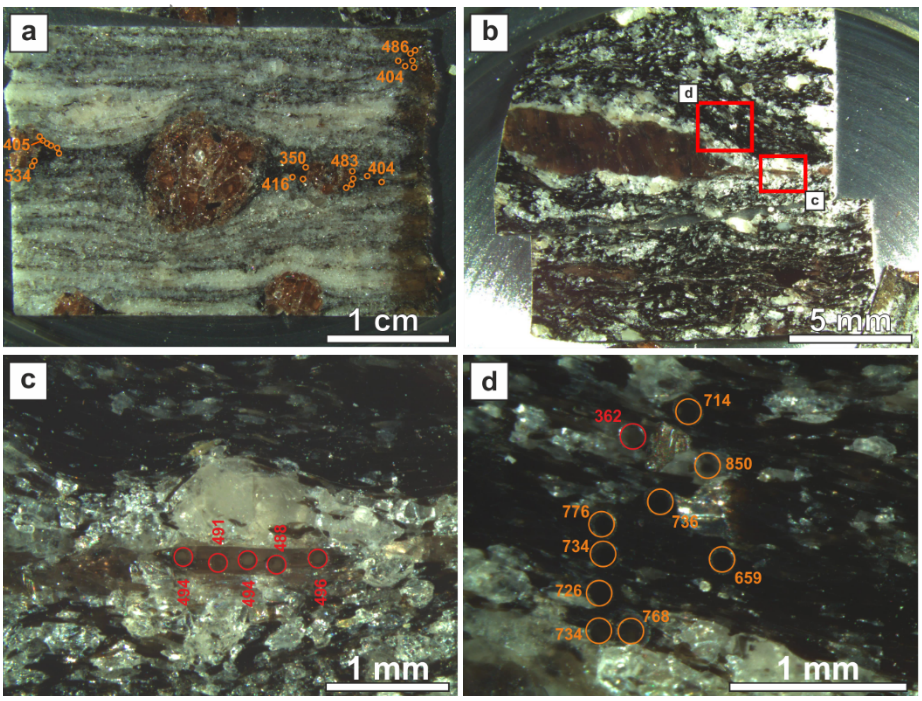

Figure SM2. Representative images of the textural positions of Bt and Wm dated with in-situ $^{40}Ar/^{39}Ar$ laser ablation geochronology. (a) Sample 240 showing the analysed Bt grains located in the strain shadows around Grt porphyroclasts. Minimum and maximum ages obtained for each microstructural site are reported. (b) Sample 251 showing the two microstructural sites investigated with is-situ laser ablation. (c) Wm-fish showing the younger dates obtained from Wm in-situ laser ablatio. (d) Bt-Wm foliation and related spot analysis showing a wide scatter in obtained dates.

Table Supplementary Material.

Table SM1. List of Perple_X solid solutions, abbreviations and relative references adopted in pseudosection calculation.

Table SM2. Sample location geographical coordinates.

Table SM1.

Solid solution name	Abbreviation of s.s. model	Abbreviation in the main text	End-members	References
Plagioclase	Pl(h)	Pl	abh, an	Newton et al. (1981)
K-feldspar	San	Kfs	san, abh	Waldbaum and Thompson (1968)
Biotite	Bi(W)	Bt	Ann, Phl, mnbi	White et al. (2014)
White Mica	Mica(W)	Wm	mu, pa, ma1_dqf, cel, fcel, fmu	White et al. (2014)
Epidote	Ep(HP11)	Ep	cz, fep	Holland and Powell (2011)
Garnet	Gt(WPH)	Grt	spss, alm, py, gr, andr_i	White et al. (2007)
Amphibole	cAmph(G)	Amp	Tr, Ts, Parg, Gl, Cumm, Grun, mrbG, Kprg, Tts	Green et al. (2016)
Chlorite	Chl(W)	Chl	daph, f3clin, ames, afchl, clin, mnchl	White et al. (2014)
Staurolite	St(W)	St	mstt, msto, fst, mnst, mst	White et al. (2014)
Cordierite	Crd(W)	Crd	mncrd, fcrd, crd, hcrd	White et al. (2014)
Chloritoid	Ctd(W)	Ctd	ctdo, fctd, mctd	White et al. (2014)
Clinopyroxene	Cpx(HP)	Cpx	esn, ccrts, cats, jd, acm, hed, di	Holland and Powell (1996); Zeh et al., (2005)

Table SM2.

Sample	Unit	GPS Coordinates (UTM WGS84)
1	L.N. Banded gneiss	70°39'17.8"N 23°44'0.5"E
2	U.N Mylonitic Eidvågeid	70°36’17.3”N 23°73’38.2”E
3	U.N. Wm-bearing Eidvågeid	70°34’30.6”N 23°41’31.6”E
4	L.N. Banded gneiss	70°34'45.6"N 23°41'25.8"E
5	L.N. Fagervik Gneiss	70°32'23.5"N 23°44'14.6"E